NASA TECHNICAL MEMORANDUM

NASA TM X-71445

NASA TM X-71445

WIND TUNNEL TESTS OF A 20 INCH DIAMETER 1.15 PRESSURE RATIO FAN ENGINE MODEL

by H. L. Wesoky and F. W. Steffen
Lewis Research Center
Cleveland, Ohio 44135

TECHNICAL PAPER proposed for presentation at Ninth Propulsion Joint Specialist Conference cosponsored by the American Institute of Aeronautics and Astronautics and the Society of Automotive Engineers
Las Vegas, Nevada, November 5-7, 1973

WIND TUNNEL TESTS OF A 20 INCH DIAMETER 1.15 PRESSURE RATIO FAN ENGINE MODEL

H. L. Wesoky* and F. W. Steffen**
Lewis Research Center
National Aeronautics and Space Administration
Cleveland, Ohio

Abstract

Aerodynamic and acoustic measurements at a typical STOL aircraft takeoff and landing velocity demonstrated that a 1.35 inlet lip area contraction ratio was superior to a 1.26 ratio at high nacelle incidence angles. Reverse thrust, obtained with a variable pitch rotor, was lower at the landing velocity, and the noise level higher, than at the static condition. High speed tests showed that, for the design cruise Mach number of 0.75, internal losses and external drag were 27 percent of the ideal fan net thrust, and propulsive efficiency was estimated to be 59 percent for an 85 percent efficient fan stage. For comparison, a similar 1.55 pressure ratio fan system would have a propulsive efficiency of 62 percent.

Introduction

Interest in the application of very high bypass ratio engines for STOL aircraft has led the NASA Lewis Research Center to investigate some possible problems of nacelle design and performance related to such engines. At cruise speed, a low pressure ratio fan has a potentially high propulsive efficiency, but, for a given thrust level, the nacelle for such a fan is large, and, thus, high drag forces can be expected. Thus a compact nacelle seems desirable. Also, because the velocity difference between the free stream and the fan discharge is small at cruise, fan duct losses have a significant effect on the net thrust. Therefore, it is important to establish the net propulsive force available from a low pressure ratio fan with a compact nacelle at cruise Mach numbers.

At takeoff and landing conditions, important areas for experimental research are the inlet performance and the interaction between the fan and nacelle at STOL aircraft speeds and high incidence angles caused by wing induced circulation. For low pressure ratio fans, there is a need to establish the levels of reverse thrust achievable with a variable pitch rotor. The variation of acoustic performance with flight speed and incidence angle should be investigated for both forward and reverse thrust.

As part of a continuing test program to study fan engines with pressure ratios from 1.15 to 1.35, engine models with 20 inch diameter 1.15 pressure ratio fans having variable pitch rotors were tested at subsonic cruise speeds in the Lewis Research Center 8- by 6-Foot Supersonic Wind Tunnel and at low speeds in the 9- by 15-Foot V/STOL Wind Tunnel. The models were tested as isolated nacelles at cruise Mach numbers from 0.60 to 0.85, and at takeoff and landing speeds from 0 to 143 feet per second. Low speed incidence angles varied from 0 to 50 degrees. Two inlet cowls having the same external contours with lip area contraction ratios of 1.26 and 1.35 were tested in both wind tunnels with two spinners. Two nozzles were tested at cruise conditions; one to obtain design point cruise performance; and the other to extend the range of inlet weight flow. For the low speed test, a fan nozzle exit area variation of 14 percent was obtained with three nozzles.

Static tests of reverse thrust performance were conducted to determine the effect of rotor blade angle. The effect of forward speed on reverse thrust performance was investigated in low speed wind tunnel tests. Reverberant noise levels were measured in the low speed tests for both the forward and reverse thrust cases.

Data to be presented here include system performance characteristics with variation of model incidence angle at a STOL aircraft takeoff and landing velocity. Low speed inlet performance will be discussed for a wide range of weight flow conditions, and the effects of rotor blade angle and forward speed on reverse thrust performance will also be indicated.

Cruise test data are presented at zero angle of attack for unit Reynold's numbers from 3.74×10^6 to 4.35×10^6 per foot. Overall force characteristics, component drags, and propulsive efficiency are presented.

Research Model and Test Facilities

A more detailed explanation of the apparatus and test procedures that can be provided here is given in reference 1 for the low speed tests and in reference 2 for the cruise tests. Some pertinent details of the apparatus and procedures will be described. Symbols are defined at the end of the paper or on the figure in question.

Fan Engine Model

A schematic drawing of the model, indicating some significant dimensions of the cruise configuration, is shown in Figure 1. The model consisted of a fan stage and nacelle, drive turbine and nozzle, and mounting pylon. The fan was driven by a 4-1/2-stage 5.9 inch diameter turbine(3) which used air as the driving fluid. Design weight flow for the turbine was 12 pounds per second for inlet conditions of 350 psia and 660° R.

Fan stage. - The 20 inch tip diameter fan stage consisted of 12 rotor blades and 32 stator blades. Hub and tip diameters were constant from rotor inlet to stator exit, and had a ratio of 0.4. The fan was designed for a 800 feet per second

* Aerospace Research Engineer, V/STOL Propulsion Technology Branch, V/STOL and Noise Division.
** Aerospace Research Engineer, Propulsion Aerodynamics Branch, Wind Tunnel and Flight Division.

(9160 rpm) tip speed, 1.15 total pressure ratio, and 66 pound per second weight flow at takeoff.[4,5] A manual adjustable pitch mechanism allowed setting of the rotor to any desired angle for forward or reverse thrust. Two rotors were built as shown in Figure 2, with the primary difference being the tip solidity. Both rotors A and B were used in the low speed wind tunnel tests. Only rotor A was used in the cruise tests. For the low speed forward thrust tests, rotor A test data will be reported for the design blade setting angle (Fig. 2); and, for the cruise tests, data will be reported for a blade angle 3 degrees higher than the design value. Rotor B test data will be reported only for a blade angle 3 degrees higher than the design value.

Inlets. - Axisymmetric fan inlets, shown in Figure 3, were designed using design procedures suggested by references 6 through 9. The external forebodies were designed for a drag divergence Mach number of 0.80 with an equivalent fan weight flow of 75.9 pounds per second at the cruise Mach number of 0.75. A single NACA 1-Series external contour[6] was used for both cowls. The proportions of the forebodies were chosen from design data given in reference 7. The lip contours between the cowl highlight and throat were elliptical, with the major axis parallel to the cowl axis and twice the length of the minor axis.[7]

The maximum cowl-to-fan diameter ratio, D_{MAX}/D_{FT}, of 1.075 was selected to keep the nacelle projected and surface areas low. Having specified the cowl highlight diameter according to the previous arguments, the maximum lip area contraction ratio, A_1/A_T, was chosen so that the inlet throat Mach number would be 0.75 at the cruise design weight flow.[8] This constraint resulted in the cowl design with the 1.35 value of A_1/A_T (Fig. 3). Another cowl lip contraction ratio, 1.26, was chosen as typical of current design practice.[8]

The maximum cowl diffuser surface angle (ϕ in Fig. 3) was set at 10 degrees as suggested by reference 9. This resulted in the values of diffuser effective cone angle given in Figure 3 which are considered conservative.[7,8] Cowl surface contours from the cowl throat to the fan face were third order polynomials with the coefficients determined from the values of the cowl radii and slopes at the throat and fan face. The two spinners had NACA 1-Series contours[6], and projected to the throats of each cowl, resulting in the minimum duct area, A_{MIN}, being slightly downstream of the cowl throats for three of the combinations of cowls and spinners, as indicated by comparison of A_1/A_T and A_1/A_{MIN} in Figure 3. This resulted in a higher average inlet throat Mach number (throat area is A_{MIN}) than was previously discussed as appropriate for the inlet with A_1/A_T of 1.35 and the long spinner.

Although not shown, cylindrical spacer rings, 1.4 inches wide, were inserted into the inner and outer walls of the inlet duct between the end of the diffuser (Fig. 3) and the fan face for all forward thrust tests in both wind tunnels. The purpose of the cowl ring was to support rake instrumentation at the fan face.

For some tests of the model with no wind tunnel flow, a standard bellmouth, with a throat diameter equal to the fan tip diameter, was used for the fan inlet.[10]

Nozzles. - Different nozzles were used for the low speed and cruise wind tunnel tests. These will be described with the appropriate discussion of results.

Instrumentation. - Fan model instrumentation pertinent to the low speed wind tunnel test data were located in the fan inlet, at the fan face, and at the fan stage exit. The inlet cowl instrumentation used here consisted of 11 static pressure taps between the cowl highlight and the fan face on the windward side of the inlet duct, with the density of pressure taps highest near the highlight. At the fan face, 6 flow rakes, each having 6 pitot tubes at centroids of equal areas, were evenly spaced around the circumference. Six other rakes, referred to as boundary layer rakes, were evenly spaced between the flow rakes on the tip side of the fan duct. Each of these rakes also had 6 pitot tubes at a distance of 0.03 to 1.11 inch from the surface. Twelve static taps were evenly spaced between the 12 rakes on the tip side of the duct at the fan face. The total pressure measurements were area averaged for evaluation of average fan inlet pressure recovery.

At the fan stage exit, six rakes similar to the flow rakes at the fan face were used. These evenly spaced rakes each consisted of 6 pitot tubes at centroids of equal areas, and a single thermocouple probe at the centroid of the annular area. Twelve static pressure taps, evenly divided between the hub and tip side of the fan duct, were located between the rake positions. Axial position of the pressure taps and pitot tubes was 0.70 inch downstream of the stator trailing edge. To avoid direct impingement of stator wakes, the static taps and rakes were located between circumferential positions of the stator blades. Rake measurements were mass averaged for evaluation of stage total pressure ratio. Pitot tubes, at both the fan face and stage exit, were not useful for the reverse thrust tests because they were directed in the conventional upstream direction.

In the cruise tests, the fan inlet total pressure was obtained from an area weighted average of total pressures measured with three six element outer wall boundary layer rakes, and wind tunnel free stream total pressure which was assumed to exist over the rest of the annulus. Fan outlet pressure was obtained from a mass weighted average of the pressures measured with three six element total pressure rakes. The fan inlet cowl suction force was obtained from a projected area weighted average of pressures measured with taps in nine element rows on the bottom, side, and top of the inlet. Pressure drag forces for other components were obtained from area weighted averages of surface static pressures obtained from rows of six taps on the bottom, side, and top of the fan and core turbine boattails; one row of sixteen taps on the external pylon; and one row of nine taps on the scrubbed (internal) pylon. The methods and equations used to obtain cruise fan weight flow, inlet pressure drag, friction drag, net propulsive force, and propulsive efficiency are contained in reference 2.

Turbine inlet pressure and temperature were obtained from an arithmetic average of two measured pressures and temperatures. Turbine outlet pressure and temperature were obtained from area weighted averages of six pressures and temperatures in the duct. Turbine weight flow was measured with a

standard sharp edged orifice.[10] These data were used to calculate turbine power and thrust.

Test Facilities

The low speed test program was conducted in the NASA Lewis Research Center 9- by 15-Foot V/STOL Wind Tunnel.[11] A photograph of the model installed in this wind tunnel is shown in Figure 4. The engine pylon was oriented in a horizontal plane and pitch motion of an aircraft installation was simulated by rotation in this plane. An axisymmetric transition piece (Fig. 4) connected the pylon to a vertical pipe through which drive air was supplied to the turbine and also supported the model. A non-metrical aerodynamic fairing, connected only to the tunnel floor, was installed around the air supply pipe to effectively eliminate aerodynamic forces on that part of the model support. The pipe was attached to an external three component force balance below the tunnel floor. Static calibration of the balance indicated a measurement accuracy of about three percent.

Acoustic data were measured with four microphones located in the wind tunnel settling chamber, about 80 feet upstream of the model. Sound pressure levels from the four microphones were selectively averaged to minimize any irregularities in the measurement. The hard walls of the wind tunnel approximated a reverberant chamber, eliminating the measurements of directional noise variation. Because of frequency selective attenuation in the reverberant situation, the spectra measured do not correspond to those that would be obtained by far-field measurement. However, the relative changes in level of forward radiated noise at a given frequency are properly associated with changes in model configuration or test condition.

The cruise tests were conducted in the Lewis Research Center 8- by 6-Foot Supersonic Wind Tunnel. For these tests, the tunnel was run over a range of Mach numbers from 0.60 through 0.85 and unit Reynolds number from 3.74×10^6 to 4.35×10^6 per foot. Figure 5 is a photograph of the nacelle installed in this wind tunnel. The nacelle, dorsal, and pylon were supported from flexure plates within a windshield. A load cell within the windshield was used to measure the thrust-minus-drag forces on the nacelle, dorsal, and pylon. The model presented a tunnel blockage of about three percent, which is considered to be acceptable for the Mach number range tested.

Low Speed Wind Tunnel Test Results

Fan Stage Performance

Fan stage performance data with the wind tunnel off were determined for several nozzle exit areas for rotors A and B with the bellmouth inlet. The word nozzle, as used here, refers to the fan aft duct of the forward thrust configuration. To obtain the desired range of operation, the fan performance required this duct to be a diffuser for the forward thrust case. Data are reported here for three such nozzles having ratios of exit area, A_e, to fan stage exit area, A_3, of 1.03, 1.11, and 1.17. Gradual straight tapered surfaces were used for the tip side of the annular ducts between the stator exit and the nozzle exit, with the largest effective cone angle being 7 degrees.[1]

With the wind tunnel drive motors off, the engine model induced tunnel velocities as high as 41 feet per second, but the effects of this on the stage performance were small. Therefore, the results with the wind tunnel off are considered representative of static conditions.

Figure 6 presents fan stage performance as measured in the wind tunnel, and as measured in a compressor test facility.[4,5] Total pressure ratio variation with weight flow was measured at 70, 90, 100, 110, and 120 percent of the fan design rotational speed. Test parameters are given here, unless otherwise stated, at equivalent standard sea level pressure and temperature conditions. Rotor B, with the higher tip solidity, performed closer to the design requirements than rotor A. Rotor A required a speed higher than 110 percent of the design value to attain the design pressure ratio. Fan stall lines were established in the compressor test facility. As shown in the figure, the stall margins with all three nozzles of the nacelle model were considered adequate.

Figure 7 shows the effects of rotational speed and nozzle area variation on fan gross thrust for rotors A and B. This thrust force was calculated using the bellmouth weight flow measurement, the average fan stage exit total temperature and pressure, and the wind tunnel static pressure. No corrections were made for duct losses downstream of the stage exit instrumentation which were believed to be small. The fan with rotor B produced thrust forces about 15 to 20 percent higher than those produced by rotor A because of its higher weight flow and pressure ratio at a specified rotational speed, as shown in Figure 6. The nozzle variation resulted in thrust variations of 10 percent or less at all fan speeds, with the strongest effect being at 120 percent speed. At this speed, the nozzle with the smallest exit area produced the highest thrust for both rotors.

System Performance Characteristics at Design Rotational Speed

All of the data reported here were obtained with a test variable sequence where tunnel velocity was first set with the model fan windmilling and the model at zero incidence angle. Then the fan rotational speed was increased to the desired level, and, finally, data were obtained at successively increasing model incidence angles. It is believed that this sequence best approximated flight conditions.

Thrust performance. - Overall model engine performance is presented from data obtained with rotor B at design rotational speed and a 143 feet per second tunnel velocity. This velocity closely corresponds to the takeoff and landing velocity proposed for commercial STOL aircraft which would use 2000 foot runways. Model incidence angle (Fig. 3), defined as the angle between the model axis and the tunnel axis, was varied from 0 to 50 degrees. The upper value was chosen because it has been shown that the effective incidence angle of nacelles mounted on current jet transport aircraft can be as much as 40 degrees, and it is expected that the closely coupled wing and engines of an externally blown flap STOL aircraft with high wing induced circulation could cause similar or even higher flow incidence angles.[12]

Because the most significant variations in performance occurred with variation of cowl lip contraction ratio, A_1/A_T, data are presented for the two cowls having contraction ratios of 1.26 and 1.35, both combined with the long spinner (Fig. 3) and the nozzle having the area ratio, A_e/A_3, of 1.17. At the fan design speed, these two configurations had about the same average inlet throat Mach numbers; 0.76 for the high contraction ratio inlet, and 0.77 for the low contraction ratio. At this high level of inlet throat Mach number, some noise suppression can be achieved by the approximation of choked flow as demonstrated in references 13 and 14. Significant amounts of noise suppression without large total pressure losses may be essential for the application of low pressure ratio fan engines in commercial aircraft.

Figure 8 presents the variation with model incidence angle, α, of fan gross thrust and net thrust measured along the model axis. The gross thrust, determined from rake measurements, decreased at incidence angles greater than 35 degrees for the low contraction ratio inlet, while no effect of increasing angle was noted for the high contraction ratio case. At an angle of 50 degrees, the gross thrust was 20 percent lower than at 35 degrees for the low contraction ratio inlet.

Net thrust was measured directly by the force balance which was aligned with the model axis. The small amount of thrust produced by the turbine was calculated from the appropriate data and subtracted from the force balance measurement. The general increase in net thrust with increasing angle was caused by the inlet momentum or ram drag component along the model axis which decreased as the angle increased. Figure 8 shows that, like the gross thrust, the net thrust decreased at angles greater than 35 degrees for the low contraction ratio inlet, while no effect of increasing angle was noted for the high contraction ratio case. At 50 degrees, the difference in net thrust between the two configurations was about 25 percent.

The effects of increasing incidence angle, α, on the fan stage total pressure ratio and weight flow are shown in Figure 9. Weight flow with the flight type inlets (Fig. 3) was determined from calibration of measured static-to-total pressure ratio at the fan face with a theoretical potential flow.[1,15] Both pressure ratio and weight flow were nearly constant at low angles for the low contraction ratio case, and at all angles for the high contraction ratio case. Reductions in both pressure ratio and equivalent weight flow occurred at high angles for the low contraction ratio inlet, which resulted in the reductions in thrust noted in Figure 8. The decrease in fan weight flow and pressure ratio noted for the low contraction ratio case suggests a condition of inlet flow distortion and cowl lip boundary layer separation.

Inlet performance. - This section presents inlet performance data for the two inlet configurations measured at the fan design speed. Figure 10 shows total pressure contours measured at the fan face for the low contraction ratio configuration at 30 degrees and 50 degrees incidence angles. Also noted on the figure are values of area averaged inlet total pressure recovery, and values of two distortion parameters. The first distortion parameter is defined as the difference between the maximum and minimum values of total pressure at the fan face divided by the area averaged total pressure. The second distortion parameter is defined as the difference between the area averaged fan face total pressure and the minimum average total pressure for any 60 degree sector of the fan face divided by the area averaged total pressure for the fan face.

As can be seen from the contour maps and the values of recovery and distortion, a large region of pressure distortion existed on the windward side of the inlet (bottom of the figure) at an incidence angle of 50 degrees (Fig. 10(b)) which was not present at 30 degrees (Fig. 10(a)), suggesting flow separation.

The axial static pressure distributions measured along the windward side of the inlet cowls, shown in Figure 11, tend to verify the boundary layer flow separation. As seen in Figure 11(a) for the low contraction ratio inlet, the minimum static pressure on the cowl surface decreased between 0 and 30 degreees incidence angle, but at 50 degrees the minimum pressure was high relative to that at 30 degrees, and a region of nearly constant static pressure existed over a long length of cowl surface. This constant static pressure is indicative of flow separation. Also at 50 degrees, the static pressure did not recover to the same level near the fan face as at 0 and 30 degrees. At zero degrees incidence angle, the minimum static pressure occurred close to the cowl throat, which is near X/X_{MAX} of 0.2 for both inlets. The minimum pressure at thirty degrees incidence angle occurred near the highlight or cowl leading edge. This minimum pressure was followed by a rapid compression and a small expansion which may have been caused by a small region of separation followed by reattachment of the boundary layer, i.e., a separation bubble, or a shock and boundary layer interaction. The separation bubble is considered a possibility because of the small region of nearly constant static pressure over a short length of surface between the highlight and cowl throat.

The comparable static pressure distributions shown in Figure 11(b) for the high contraction ratio case indicated no complete flow separation at any incidence angle. Again, as for the previous case, the minimum surface pressure decreased between 0 and 30 degrees, but continued to decrease beyond 30 degrees to the very low value shown for 50 degrees which corresponds to a peak Mach number of about 2.1. At 0 degrees, the minimum pressure occurred near the cowl throat, and, at 30 and 50 degrees, the minimum pressure occurred near the highlight. Near the highlight, at 0 and 30 degrees, the pressure distributions for the high contraction ratio cowl indicate regions of compression followed by expansion. A possible cause for this pressure distribution could be the geometry of the cowl leading edge where a sudden change in surface curvature occurred at the intersection of the external forebody (with a small radius of curvature) and the lip (with a relatively large radius of curvature). This effect of curvature has been theoretically demonstrated in reference 16.

Acoustic performance. - The effects of inlet geometry and incidence angle variation on the system noise level as measured in the upstream chamber of the tunnel are indicated in Figure 12. Sound pressure level spectra resulting from one-third octave band analysis are shown for the two inlet configurations and test parameters previously consid-

ered. The blade passing frequency (BPF) and a multiple (2 BPF) are noted on the figure. Also shown is the background noise spectrum which resulted from the wind tunnel operation alone. As indicated in Figure 12(a), the background noise was from 3 to 30 decibels below the spectra obtained with model operation, except at frequencies below about 400 hertz where the noise levels were about equal.

Noise data for the high contraction ratio inlet case indicated relatively small increases in noise level across the entire frequency range between 0 and 50 degrees incidence angle. At the blade passing frequency, which was dominant, the increase was about 4 decibels. The spectra for the three angles shown were similar in shape with sharp peaks near the blade passing frequency and at two times this frequency. The observed increases in upstream radiated noise level with increasing incidence angle correlated with small increases in inlet flow distortion.

Noise data for the low contraction ratio inlet case (Fig. 12(b)) also indicated modest increases between 0 and 30 degrees, with about a 2 decibel increase at the blade passing frequency. However, between 30 and 50 degrees, a large increase in noise level occurred over a broad frequency range. At the blade passing frequency, the increase was about 8 decibels, and over a significant range of lower frequencies the increase was about 15 decibels. The broadband nature of the noise increase nearly eliminated the peaks at the blade passing frequency and its multiple. The result correlates with the inlet flow separation and large flow distortion demonstrated previously for the low contraction inlet configuration. For 50 degrees incidence angle, the low contraction ratio configuration had a noise level about 5 decibels higher than the high contraction ratio case at the blade passing frequency.

The increases of upstream measured reverberant noise levels demonstrated in this experiment for increasing model incidence angle agree with those demonstrated in reference 14 for an unchoked inlet. Increases in noise level that occurred without large flow distortion, as for the high contraction ratio inlet (Fig. 12(a)), could be important for a commercial STOL aircraft which will be required to operate under stringent noise regulations.

Variation of Inlet Performance with Weight Flow

The previous discussion dealt with a single fan operating condition and clearly defined the importance of inlet design on system performance. In this section, inlet performance data are presented as a function of weight flow at a tunnel velocity of 143 feet per second to demonstrate performance over a wider range of operating conditions, and to examine the effects of fan rotor and nozzle variation on the performance.

High contraction inlet with long spinner. - Figure 13(a) shows the variation of inlet total pressure recovery with fan equivalent weight flow for the configuration with cowl contraction ratio, A_1/A_T, of 1.35 and the long spinner. Data were obtained with both fan rotors over a wide range of weight flow and model incidence angle. Noted with the data are the corresponding fan rotational speeds for each case, and the inlet average throat Mach number at zero incidence angle for a few cases.

Figure 13(b) shows the variation of a circumferential flow distortion parameter previously defined with weight flow for the same case as Figure 13(a). No effect of the variation of fan rotor design can be discerned from either figure. At zero incidence angle, a general reduction in pressure recovery (Fig. 13(a)) resulted from increasing weight flow. This reduction was associated with increased viscous losses and boundary layer thickness which occurred uniformly around the fan circumference causing a radial flow distortion, but no significant circumferential distortion as can be seen in Figure 13(b). The increased boundary layer thickness for the higher weight flows resulted from an increased adverse pressure gradient between the cowl lip and the fan face, and the increase of the Mach number level in the inlet duct.

At 30 degrees incidence angle, a significant increase in circumferential flow distortion occurred for weight flows greater than 40 lb/sec-ft^2, where noise suppression due to high throat Mach number can occur. The pressure recovery values were somewhat lower than at zero incidence angle.

For 0 and 30 degrees, the inlet performance decreased in a continuous manner with increasing weight flow. At 40 and 50 degrees incidence angles, narrow ranges of weight flow existed where inlet performance was good, but on either side of these ranges, high distortion and low recovery occurred. The range of weight flow for which good performance occurred was wider at 40 degrees than at 50 degrees. The primary region of flow distortion in all cases was on the windward side of the inlet.

The relatively good performance demonstrated by the inlet over a narrow range of weight flow at the highest incidence angles is significant. At low weight flow, poor performance was obviously caused by separation of flow from the cowl lip. This may be important for low engine throttle setting operation, which is considered during an aircraft landing maneuver. At higher weight flows, where the performance improved, the character of the boundary layer must have changed to allow the flow to traverse the adverse pressure gradient without separating. At even higher weight flows, where the performance decreased again, a possible cause could have been strong shock and boundary layer interaction. Further tests should be conducted to understand the flow structure which occurred, and to determine the effect of model size on the inlet performance.

For the 36 lb/sec-ft^2 design weight flow of the 1.15 pressure ratio fan, the inlet of Figure 13 produced small total pressure losses and low distortion for model incidence angles between 0 and 40 degrees. At 50 degrees the performance was undefined, but, at 37 lb/sec-ft^2 (slightly higher than the design value), the performance was satisfactory. At both higher and lower weight flows, the performance at 50 degrees decreased.

High contraction inlet with short spinner. - Figure 14 shows the same parameters for the same cowl and fan rotor configurations as Figure 13, but with the short spinner. The same general observations made for the previous inlet configuration can also be made for this case. A possible effect of rotor variation did occur at 50 degrees incidence angle between 40 and 41 lb/sec ft^2 weight flow.

However, it is not certain what caused the lower pressure recovery and higher distortion for the rotor A configuration, and it could be surmised that experimental error or a boundary layer instability was the reason. Data for 0 and 30 degrees incidence angles were very similar to those indicated for the inlet with the long spinner. At 40 and 50 degrees incidence angle, however, good performance was obtained over a narrower range of weight flow for the short spinner case than for the long spinner case. At high angles, the long spinner may have provided some directivity to the flow which helped to keep the cowl surface boundary layer from separating at weight flows where separation did occur with the short spinner.

It should be noted that, in the region of weight flow required to obtain the high throat Mach numbers (greater than about 0.80) where large amounts of noise suppression can occur[13,14], the performance of both inlet configurations was sensitive to throat Mach number and incidence angle. As previously shown in Figure 12 for design rotational speed, even without complete flow separation, increased noise levels resulted from the small flow distortions associated with this operating condition at high incidence angles.

At the design weight flow of 36 lb/sec ft^2 for the 1.15 pressure ratio fan, the inlet with the short spinner clearly performed well at 0 and 30 degrees model incidence angles. Because of the gap between data points near the design weight flow, it is not clear that this inlet performed satisfactorily at 40 degrees, but, because the low contraction ratio inlet (to be discussed next) did perform well, it is believed proper to assume that the high contraction ratio inlet produced similar performance. At 50 degrees, the performance was not defined at the design weight flow, but, as for the long spinner case, it is clear that, at weight flows near the design value, flow separation would occur.

Low contraction inlet. - Figure 15 gives the performance characteristics of the 1.26 contraction ratio inlet with the short spinner. Fan rotor A was used with two nozzle area ratios, A_e/A_3, of 1.03 and 1.11. No effect of the nozzle area variation (fan operating point) on inlet performance was discerned from these data. For incidence angles up to 30 degrees, total pressure losses and flow distortion were small over the entire range of weight flow. At 40 and 50 degrees, the data points were connected according to the progression of fan speed which occurred at zero incidence angle for the corresponding progression of weight flow. This accounts for the somewhat erratic appearance of the lines connecting data points for these angles where the weight flow measurement was not as accurate as at lower angles because of flow distortion. At 40 degrees incidence angle, a range of weight flow between 36 and 40 lb/sec-ft^2 existed where the performance remained satisfactory. However, for higher and lower weight flows, separation occurred, resulting in large pressure loss and distortion. The possible causes of this occurrence are the same as those previously discussed for the other inlets. At 50 degrees, the flow was completely separated from the inlet lip over the entire range of weight flow.

At the 36 lb/sec-ft^2 design weight flow for the 1.15 pressure ratio fan, the low contraction ratio inlet had a slightly higher pressure recovery than either of the high contraction ratio inlets at incidence angles up to 30 degrees. At 30 degrees, the difference was about 0.001. This probably resulted from the shorter duct length and lower throat Mach number of the low contraction ratio inlet. At 40 degrees, the performance was satisfactory for the design weight flow, but, at 50 degrees, as stated previously, the performance was poor at all weight flows.

To insure satisfactory performance over a wide range of weight flow at high incidence angles, the results of Figures 13, 14, and 15 indicate that a lip contraction ratio, A_1/A_T, of 1.35 or greater would be necessary on the windward side of the inlet if all other geometric characteristics of the inlet were similar to those used here. Increased losses will occur with increasing throat Mach number, with increasing sensitivity to throat Mach number as the choked flow condition is approached.

Reverse Thrust Performance

Reverse thrust data were obtained only with fan rotor A. The first objective of this part of the test program was to determine the rotor blade angle which provided the best reverse thrust performance. Relative to the forward thrust blade setting angle, two types of blade angle change were tested. The first type involved rotation of the blades through the "stopped rotor feather" position (Fig. 2). In this approach, the normal trailing edge of the blades became the leading edge for reverse thrust application and the blade camber was proper. The second type required rotation through the flat position of the blades. This resulted in the normal leading edge as the leading edge for reverse thrust application, but with reverse camber.

Thrust data. - Figure 16 shows thrust data for three blade angles with the wind tunnel off and a bellmouth nozzle. The reverse thrust blade angles presented provided the maximum reverse thrust at high fan speed. More details of the effect of blade setting angle on reverse thrust are given in reference 1. For comparison, the variation in net forward thrust produced by the fan at its design rotor angle is also shown.

The reverse thrust forces obtained with blade rotation through the feather position were greater than those obtained by rotation through the flat position, ranging from 1.5 times at 70 percent fan speed to about 1.9 times at 120 percent fan speed. These large differences in thrust levels between the two types of reverse thrust blade angle settings were observed for all blade angles tested. It therefore appears that having the correct blade camber for reverse thrust was more important than having the correct blade leading edge.

A direct comparison of the absolute values of measured reverse thrust to the forward thrust at the design rotor angle shows that, for the case where the blades were rotated through the feather position, the reverse thrust was about 50 percent of the forward thrust at 70 percent fan speed, and 60 percent of the forward thrust at 120 percent fan speed. The values might be somewhat different for the true static case because of the small effects of induced tunnel flow on the data presented.

The effect of wind tunnel velocity on reverse thrust performance (reverse through feather) at

110 percent fan speed is presented in Figure 17 where the net thrust variation is shown for a range of velocities from near static to a typical STOL aircraft landing speed. The conical nozzle used to obtain these data (Fig. 17) was considered appropriate for the reverse thrust case. Shown for comparison are forward thrust data for the same fan speed. At the lowest velocity indicated in Figure 17, where the wind tunnel was off and flow was induced by the model, the reverse thrust force was about the same as that previously shown in Figure 16. This indicates that the conical nozzle, used with tunnel flow, performed similarly to the bellmouth nozzle at near static conditions.

An increase in tunnel velocity caused a reduction of reverse thrust. The rate of reduction increased significantly above 120 feet per second velocity, resulting in the reverse thrust at 140 feet per second being about 50 percent of that with the wind tunnel off. Comparison with the forward thrust data shows that the thrust lapse curves have similar trends. At a tunnel velocity of 140 feet per second, the reverse thrust was about 35 percent of the comparable forward thrust. A possible reason for the reverse thrust lapse with increasing tunnel velocity was a reduction in reversed fan weight flow caused by reduced pressure recovery in the reverse thrust nozzle and the interaction of the tunnel flow and reversed fan jet.

Acoustic data. - Upstream measured reverberant noise performance for a typical reverse thrust condition is shown in Figure 18 for 110 percent fan speed and two tunnel velocities. An increase in noise level across the entire frequency range occurred between the lower velocity, which was obtained with the wind tunnel off, and the typical STOL aircraft landing velocity. At the blade passing frequency, the increase was about 7 decibels, with somewhat larger increases occurring at other frequencies. The increase in noise level over a broad band of frequencies was attributed to reverse flow inlet performance, and interaction between the tunnel flow and reverse fan jet. A significant increase in overall sound pressure level could result from this broad band change in noise spectra, assuming no frequency selective attenuation. It is believed that none of the noise increase was associated with the wind tunnel operation. Forward thrust noise data, measured under similar conditions, indicate that the noise of the wind tunnel had no effect on the results indicated here.(1)

A comparison of the reverse thrust noise data presented here with forward thrust noise data given in reference 1 for 120 percent fan speed indicates that forward radiated reverse thrust noise levels may be higher because of high sound pressure levels over a broad frequency range. At the typical STOL aircraft landing velocity noted previously, noise levels at the blade passing frequencies were approximately equal, but at both higher and lower frequencies, the broadband spectrum for reverse thrust was as much as 10 decibels higher than that for forward thrust.

High Speed Wind Tunnel Test Results

Three of the inlets tested at low speed were also tested at high speed, or cruise, conditions. They were the 1.26 contraction ratio cowl with the short spinner, and the 1.35 contraction ratio cowl with both the long and short spinners.

Nozzles used in the cruise investigation, and their pertinent geometric parameters, are shown in Figure 19. The exit areas listed in the figure are the annular exit flow areas. Fan nozzle 1 was the cruise nozzle and was sized to give an inlet mass flow ratio, A_0/A_{MAX}, of approximately 0.65 at a free stream Mach number of 0.75 with a fan pressure ratio of 1.15. At design cruise conditions (0.75 Mach number and 1.15 fan pressure ratio), the nozzle pressure ratio was 1.66. Fan nozzle 2 had a larger annular flow exit area than nozzle 1, and was used only to extend the range of inlet mass flow ratio over which inlet pressure drag data were obtained. The core turbine nozzle (also used in the low speed wind tunnel tests) had a constant area duct. The turbine nozzle boattail was contoured essentially the same as the fan nozzle boattail. The turbine nozzle boattail was scrubbed by the fan jet which had a flow Mach number of about 0.9 at the design cruise condition.

The cruise tests were made over a range of Mach numbers from 0.60 to 0.85 at zero incidence angle. Overall thrust and drag forces, component pressure drag forces, and the propulsive efficiency of the fan-nacelle system will be discussed in the following sections.

Overall Forces

A comparison of the total propulsive force coefficients of the nacelle, including the core turbine thrust, obtained with the three inlets, is shown in Figure 20. These inlets differed primarily in internal contours (Fig. 3) and were not expected to give large differences in cruise performance. At a fan pressure ratio of approximately 1.1, where the fan flow rates were low, no differences in propulsive force were noted across the Mach number range. However, at a fan pressure ratio of approximately 1.15, where the fan flow rates were high, the inlet with the 1.35 contraction cowl and the long spinner gave somewhat lower performance over the Mach number range. The performance loss probably was caused by the inlet losses associated with high internal inlet velocities. At Mach 0.75 and above, the flow in the inlet actually choked. Thus, the inlet with the 1.35 contraction ratio cowl and the long spinner would not be acceptable for cruising flight. Use of the short spinner with the 1.35 contraction cowl alleviated choking and resulted in an acceptable inlet. Thus, the inlet composed of the 1.35 contraction ratio cowl and the short spinner was found to meet both the high and low speed requirements.

The pressure gradients near the highlight of the 1.35 contraction ratio cowl were of such a nature that an accurate calculation of the cowl suction force using the available instrumentation was impossible. Conversely, the gradients on the 1.26 contraction ratio cowl were well defined by the instrumentation and it was possible to calculate cowl suction force and inlet pressure drag. Since the 1.35 contraction ratio cowl with the short spinner and the 1.26 contraction ratio cowl with the short spinner had the same performance characteristics, as indicated in Figure 20, data taken with the latter inlet are considered to be representative of either inlet and are used in all the remaining figures.

The overall measured performance of the fan/nacelle over the Mach number range is shown by the

lowermost curve in Figure 21. These data are for a constant fan pressure ratio of 1.15. Mass flow ratio varied from 0.700 at Mach 0.60 to 0.645 at Mach 0.85. This curve gives the fan/nacelle net propulsive force (load cell force less the calculated core turbine thrust) ratioed to the ideal fan net thrust. The ideal fan net thrust is the net thrust calculated from the fan stage total pressure ratio and weight flow with no internal losses. A breakdown of the loss in net thrust from the ideal value is also presented in Figure 21. The external pressure drag, determined from an integration of measured surface static pressures, and the calculated flat plate friction drag were added to the lowermost curve to obtain the two intermediate curves. The uppermost curve was obtained by calculating a net thrust based on the measured fan outlet total pressure. For a particular fan pressure ratio, this value reflected the inlet loss. The difference between the two upper curves was considered to be the fan nozzle internal loss.

At Mach 0.75, only 73 percent of the ideal fan net thrust was available for propulsion. The inlet internal loss accounted for about 2 percent of the ideal fan net thrust and the nozzle internal loss an additional 5 percent, resulting in a total internal loss of 7 percent. The calculated flat plate friction drag[2] and the measured pressure drag each accounted for 10 percent of the ideal fan net thrust for a total drag force equal to 20 percent of the ideal fan net thrust. The rapid decrease in fan/nacelle net propulsive force ratio above Mach 0.8 was due to divergence of the inlet pressure drag.

Calculated overall drag coefficients for the nacelle, dorsal, and pylon are shown over the test Mach number range in Figure 22. The fan stage total pressure ratio was held constant at 1.15 and the mass flow ratio varied from 0.700 at Mach 0.60 to 0.645 at Mach 0.85. A drag coefficient line equivalent to 25 percent of the ideal fan net thrust is shown for reference. At Mach 0.75, the drag coefficient for the combined nacelle, dorsal, and pylon was approximately 0.052. Flat plate friction drag was about half of the total drag, or in other words, friction drag and pressure drag were about equal for this nacelle, dorsal, and pylon. Above Mach 0.75, the pressure drag increased rapidly due to divergence of the inlet pressure drag.

At Mach 0.75, a calculation of friction drag was made using the velocities determined from pressure measurements on the fan cowl. These velocities slightly increased the friction drag above flat plate values but should have little effect on the total drag values presented.

Pressure Drag Components

Pressure drag coefficients are shown in Figure 23. As in the previous figure, these coefficients are based on free stream dynamic pressure and nacelle maximum cross-sectional area. The data is presented for a constant fan pressure ratio of 1.15. A drag coefficient line equivalent to 5 percent of ideal fan net thrust is included for reference.

Inlet pressure drag is defined as the difference between additive drag and cowl suction force. The inlet pressure drag coefficient, Figure 23(a), was slightly negative from Mach 0.6 through 0.75. Results obtained from potential flow equations, such as described in reference 17, have indicated that inlet pressure drag can be reduced by the close coupling of a boattail. The low pressure on the boattail can reduce the pressure on the fan cowl and increase the cowl suction force. Drag rise occurred at approximately the design drag divergence Mach number of 0.8.

The boattail drag coefficients are shown in Figure 23(b). The fan boattail pressure drag was the largest component of pressure drag at Mach 0.75. Its value at Mach 0.75 was somewhat higher than that reported for boattails preceded by long cylindrical sections such as in reference 18. Above Mach 0.75, the boattail pressure drag coefficient decreased slightly as the inlet pressure drag coefficient increased rapidly. These results for the boattail again imply a possible interaction between the fan inlet and nozzle boattail flow fields. At Mach 0.75, the drag coefficient for the core turbine nozzle boattail, which was preceded by a long cylindrical section, did agree well with the values in reference 18.

Both the scrubbed and external pylon pressure drag were considerably higher than typical airfoil pressure drag (which would have been essentially zero). Together, they accounted for a drag force equal to about 5 percent of the fan net thrust. Some of the pylon drag resulted from failure of the flow to fully recompress on the rather abrupt closure of the pylon afterbody. Hopefully, much of this drag could be eliminated in a redesigned pylon.

Inlet pressure drag. - The variation of inlet pressure drag coefficient with mass flow ratio is shown in Figure 24 for Mach 0.75 and 0.85. To extend the range of mass flow ratio, data obtained with both nozzles 1 and 2 are shown. This change in nozzle geometry appears to have had a negligible effect on the inlet drag as evidenced by a small change in the drag coefficient level when the two sets of data overlap. At Mach 0.75, the drag coefficient approached a minimum value of less than zero as the mass flow ratio was increased. At Mach 0.85, the inlet choked before a minimum value was reached.

The additive drag and cowl suction force coefficients (which are algebraically summed to obtain the inlet pressure drag coefficient) are shown in Figure 25 as a function of mass flow ratio. Data for Mach 0.75 and 0.85 are presented in parts (a) and (b), respectively. At all mass flow ratios shown, the additive drag coefficient was significantly higher at Mach 0.85 than at Mach 0.75, and the cowl suction coefficient was considerably less at Mach 0.85 than at Mach 0.75. At Mach 0.75, the cowl suction coefficient exceeded the additive drag coefficient at mass flow ratios greater than 0.64, while at Mach 0.85, the cowl suction coefficient was considerably below the additive drag coefficient at any of the mass flow ratios shown.

A further explanation of these data variations is obtained by examination of the cowl pressure distributions. The cowl pressure coefficient distributions at Mach 0.75 and 0.85, both at a mass flow ratio of 0.658, are presented in Figure 26. The cowl suction coefficient at a particular Mach number is the difference between the area above the curve, labeled thrust, and the area below the curve, labeled drag. The stagnation and highlight pressure coefficients are less at Mach 0.75 than at

Mach 0.85 and thus the area under the curve is less at Mach 0.75 than at Mach 0.85. Also, the minimum pressure coefficients are lower at Mach 0.75 than at Mach 0.85, and thus the area above the curve was slightly greater at Mach 0.75 than at Mach 0.85. This was true even though the pressure coefficients at Mach 0.85 remained nearly constant at the maximum negative value, indicating a possible separation of the flow from the cowl. These distributions were typical for the entire range of mass flow ratios tested at Mach 0.75 and 0.85.

Fan nozzle boattail pressure drag. - Fan nozzle no. 1 boattail pressure drag coefficients are shown in Figure 27 as a function of nozzle pressure ratio for all inlet configurations. At all free stream Mach numbers, the drag coefficient decreased slightly with increasing nozzle pressure ratio, although the range of nozzle pressure ratios at each Mach number was quite limited. The drag coefficient also decreased with increasing Mach number. These results do not agree with the results shown in reference 18 when an increase in boattail drag was noted when the nozzle pressure ratio was increased from 1.5 to 2.0 at a constant Mach number of 0.85. The disagreement may result from the differences in forebody geometry as mentioned previously.

The fan nozzle boattail pressure distribution obtained at a free stream Mach number of 0.75 and the nozzle pressure ratio (1.67) resulting from a fan pressure ratio of 1.15 is presented in Figure 28. The first pressure coefficient on the fan boattail agreed well with the last pressure coefficient on the fan cowl which was located 1.01 maximum nacelle diameters upstream. The boattail pressure coefficient then increased continuously from the pressure tap nearest the maximum nacelle diameter to the tap nearest the fan nozzle exit plane. Unlike the pressure distributions often seen on boattails preceded by long cylindrical forebodies, the pressure distribution did not indicate a sharp flow overexpansion associated with the boattail juncture. These results, together with the inlet drag levels, point up the importance of testing engine/nacelle models rather than separate components.

Propulsive Efficiency

In Figure 29, the propulsive efficiency of the nacelle at a constant fan pressure ratio of 1.15 is shown as a function of free stream Mach number. The propulsive efficiency was defined as the experimental fan net thrust minus the nacelle and pylon drag times the free stream velocity divided by the power input to the fan. The experimental fan net thrust minus the nacelle and pylon drag was obtained by subtracting the core thrust from the load cell force. The power to the fan stage was obtainby by dividing the stream power of the fan by several assumed values of fan stage efficiency. Assumed values were used because the measured efficiency of the experimental fan stage was not typical of the efficiency of a highly developed fan. At Mach 0.75, the propulsive efficiency with a 100 percent efficient fan was 70 percent and with a more realistic value for fan efficiency of 85 percent, the propulsive efficiency dropped to 59 percent. For comparison, the propulsive efficiency of a 1.55 pressure ratio fan without duct losses (e.g., without noise suppression splitters) would be about 62 percent using the same flight conditions and nominal values of drag coefficient and specific weight flow. Thus, on the basis of propulsive efficiency, the 1.15 pressure ratio system is only a few percentage points below present day systems. Reduction of pylon drag would reduce this difference to an even smaller value.

For high propulsive efficiency, the nacelle should have a low drag coefficient and the nacelle/fan system should handle as large an equivalent weight flow per unit nacelle area as possible. The relationship of these quantities is shown in Figure 30 for a 1.15 pressure ratio fan/nacelle system operating at a Mach number of 0.75 at 25,000 feet. A fan stage efficiency of 0.85 was assumed. The curves were obtained by plotting the equation for analytical propulsive efficiency which is

$$\eta_{PA} = \frac{(\text{Net Thrust-Drag})V_0}{\text{Power to Fan}} = \frac{\left(\frac{V_e}{g} - \frac{V_0}{g} - \frac{C_D q_0}{\left(\frac{W\sqrt{\theta_2}}{\delta_2 A_{MAX}}\right)\frac{\delta_2}{\sqrt{\theta_2}}}\right)V_0}{\frac{c_p T_0}{\eta_F}\left[\left(\frac{P_3}{P_2}\right)^{2/7} - 1\right]} \qquad (1)$$

A point based on the experimental drag coefficient (0.052) and the experimental specific equivalent flow rate (30.1 lbs/sec-ft^2) is shown. The experimental value with fan duct losses is also shown. As seen in Figure 30 and equation (1), propulsive efficiency at a given cruise condition and fan stage pressure ratio can be improved by reducing the overall drag coefficient and increasing the value of weight flow per unit of frontal area. The specific equivalent weight flow can be further expanded as follows:

$$\frac{W\sqrt{\theta_2}}{\delta_2 A_{MAX}} = \left(\frac{W\sqrt{\theta_2}}{\delta_2 A_2}\right)\frac{A_2}{A_{MAX}} = \left(\frac{W\sqrt{\theta_2}}{\delta_2 A_2}\right)\frac{\left(1 - \left(\frac{D_{FH}}{D_{FT}}\right)^2\right)}{\left(\frac{D_{MAX}}{D_{FT}}\right)^2} \qquad (2)$$

The term $W\sqrt{\theta_2}/\delta_2 A_2$ is a function of fan design and should be maximized. The term D_{FH}/D_{FT} is also a function of fan design and should be minimized. The experimental value of $W\sqrt{\theta_2}/\delta_2 A_2$ was 41.4 lb/sec-ft^2 (fan face Mach number of 0.6) and the experimental value of D_{FH}/D_{FT} was 0.4. The term D_{MAX}/D_{FT} is a function of nacelle design and together with C_D should be minimized. For the experimental nacelle, the value of D_{MAX}/D_{FT} was only 1.075. Any method of reducing C_D which would also increase D_{MAX}/D_{FT} should be carefully examined to determine the net effect on propulsive efficiency.

Summary of Results

Tests of a 20 inch diameter 1.15 pressure ratio fan engine model with a variable pitch rotor conducted at representative STOL aircraft takeoff and landing velocities with an isolated nacelle

configuration in a low speed wind tunnel produced the following major results:

1. At design rotational speed and below a model incidence angle of about 35 degrees, the aerodynamic and acoustic performance of two configurations having inlet lip area contraction ratios of 1.26 and 1.35 were similar. At higher incidence angles, performance of the low contraction ratio configuration decreased. At 50 degrees, its net thrust was about 25 percent lower and its forward radiated reverberant noise level was about 5 decibels higher at the blade passing frequency than the high contraction ratio inlet case. Reduced performance was caused by boundary layer flow separation from the inlet lip.

2. Each of the inlet configurations had a narrow range of weight flow where, at high incidence angles (40 to 50 degrees), the inlet performance was satisfactory, but, at both higher and lower weight flows, cowl surface boundary layer separation caused a reduction in performance.

3. High inlet throat Mach numbers, as might be required for noise suppression by approximation of choked flow, resulted in a reduction of inlet performance at all incidence angles, including the low angles (0 to 30 degrees) where the performance was satisfactory for lower throat Mach numbers.

4. Variation of fan rotor design or nozzle exit area did not significantly affect inlet performance.

5. Reverse thrust forces obtained with fan rotor rotation through the feather blade angle were 1.9 times larger than with blade rotation through the flat blade angle at the highest fan speed and near static wind tunnel conditions. At a typical landing velocity, reverse thrust force was 50 percent lower, and forward radiated reverberant noise level was 7 decibels higher at the blade passing frequency than at a near static condition.

Tests of the engine model at typical cruise conditions in a high speed wind tunnel produced the following principal results:

1. At Mach 0.75, the net propulsive force of the nacelle (excluding turbine thrust) was 73 percent of the ideal fan net thrust. Internal losses amounted to 7 percent, and drag amounted to 20 percent of the ideal fan net thrust. The drag coefficient (based on wind tunnel dynamic pressure and maximum nacelle cross sectional area) for the nacelle, dorsal and pylon was about 0.052. Drag divergence occurred at the inlet design value of 0.80.

2. Acceptable cruise performance was obtained with the inlet having a cowl lip area contraction ratio of 1.26 and a spinner which projected to the cowl throat. Performance of the inlet with a 1.35 contraction ratio cowl and a spinner projecting to its throat was unsatisfactory because of losses associated with choked inlet duct flow at the cruise condition of Mach 0.75. Acceptable performance was obtained with the 1.35 contraction ratio inlet cowl when a shorter spinner, which did not cause choked flow, was used. The two cowls had the same external contours.

3. Inlet pressure drag was negative at cruise conditions. Also, the fan boattail pressure drag was higher than estimated from isolated boattail drag data, and decreased slightly as the inlet drag diverged. These results, together with available potential flow analyses, suggested an interaction of the inlet and boattail flow fields and pointed up the need for complete nacelle testing.

4. At Mach 0.75, the propulsive efficiency of the fan/nacelle system, assuming an 85 percent efficient fan stage, was 59 percent. It was shown that both a low drag coefficient and a high ratio of equivalent flow rate-to-maximum nacelle frontal area were necessary to achieve high propulsive efficiency.

5. The experimental 1.15 pressure ratio fan nacelle system achieved a high specific equivalent flow rate by using a thin walled nacelle, a low hub-to-tip ratio fan and a high fan face Mach number. The propulsive efficiency of this system was about 3 percentage points less than the corresponding efficiency calculated for a similar 1.55 pressure ratio system operating at the same flight conditions.

Symbols

A	Area
A_{MAX}	Maximum nacelle cross section area
BPF	Blade passing frequency
C_D	Drag coefficient, $Drag/q_o A_{MAX}$
C_P	Pressure coefficient
c_p	Specific heat
D	Diameter
F	Model net thrust (force measured by balance minus core turbine thrust)
F_{CORE}	Calculated thrust of core turbine
F_{ID}	Ideal net thrust of fan stream with no inlet or outlet duct losses
g	Gravitational constant
M	Mach number
P	Total pressure
p	Static pressure
q	Dynamic pressure
R	Radius
T	Total temperature
V	Velocity
W	Fan weight flow
X	Model axial length
α	Model incidence angle
β	Fan rotor blade setting angle
δ	Ratio of total pressure to standard sea level pressure

η_F	Fan stage adiabatic efficiency
η_P	Measured propulsive efficiency
η_{PA}	Analytical propulsive efficiency
θ	Ratio of total temperature to standard sea level temperature

Subscripts

AV	Average
e	Fan nozzle exit annulus
F	Fan
FH	Fan hub
FT	Fan tip
MAX	Maximum
MIN	Minimum
MIN60	Minimum over any 60 degree interval
PROJ	Projected annular area between local pressure tap and D_{MAX}
T	Cowl throat
0	Wind tunnel free stream
1	Cowl highlight
2	Fan face
3	Fan stage exit

References

1. Wesoky, H. L., Abbott, J. M., Albers, J. A., and Dietrich, D. A., "Low Speed Wind Tunnel Tests of a 50.8 Centimeter (20 Inch) 1.15 Pressure Ratio Fan Engine Model," Technical Memorandum to be published, NASA, Cleveland, Ohio.

2. Steffen, F. W., "Performance of an Isolated 1.15 Pressure Ratio Turbofan Engine Simulator at Mach Numbers from 0.6 to 0.85," TM X-68263, 1973, NASA, Cleveland, Ohio.

3. Wasserbauer, C. A., "Calculated Performance of a 4-1/2-Stage 15.0 Centimeter (5.9-In.) Diameter Turbine Designed for a 50.8-Centimeter (20.0 In.) Turbofan Simulator," TM X-2822, 1973, NASA, Cleveland, Ohio.

4. Osborn, W. M., and Steinke, R. J., "Performance of a 1.15 Pressure Ratio Axial-Flow Fan Stage With a Blade Tip Solidity of 0.5," Technical Memorandum to be published, NASA, Cleveland, Ohio.

5. Kovich, G., "Overall and Blade Element Performance of a Low Pressure Ratio Low Blade Tip Speed STOL Fan Compressor Stage," Technical Memorandum to be published, NASA, Cleveland, Ohio.

6. Baals, D. D., Smith, N. F., and Wright, J. B., "The Development and Application of High-Critical-Speed Nose Inlets," Report 920, 1948, NACA, Hampton, Virginia.

7. Hancock, J. P., and Hinson, B. L., "Inlet Development for the L-500," Paper 69-448, June 1969, AIAA, New York, N. Y.

8. Douglass, W. M., "Aerodynamic Installation of High-Bypass-Ratio Fan Engines," Paper 660732, Oct. 1966, SAE, New York, N. Y.

9. Fasching, W. A., "Air Force Advanced Lift Fan and Lift/Cruise Fan Demonstrator Program," R69AEG150, Vol. 2, AFAPL-TR-69-7, Vol. II, Feb. 22, 1969, General Electric Co., Cincinnati, Ohio.

10. Anon., ASME Power Test Codes, Supplement on Instruments and Apparatus, Part 5, Chapter 4, 1959.

11. Yuska, J. A., Diedrich, J. H., and Clough, N., "Lewis 9- by 15-Foot V/STOL Wind Tunnel," TM X-2305, 1971, NASA, Cleveland, Ohio.

12. Albers, J. A., "Predicted Upwash Angles at Engine Inlets for STOL Aircraft," TM X-2593, 1972, NASA, Cleveland, Ohio.

13. Klujber, F., "Results of an Experimental Program for the Development of Sonic Inlets for Turbofan Engines," Paper 73-222, Jan. 1973, AIAA, New York, N. Y.

14. Miller, B. A., and Abbott, J. M., "Low-Speed Wind-Tunnel Investigation of the Aerodynamic and Acoustic Performance of a Translating-Centerbody Choked-Flow Inlet," TM X-2773, NASA, Cleveland, Ohio.

15. Albers, J. A., "Theoretical and Experimental Internal Flow Characteristics of a 13.97 Centimeter-Diameter Inlet at STOL Takeoff and Approach Conditions," TN D-7135, 1973, NASA, Cleveland, Ohio.

16. Albers, J. A., and Miller, B. A., "Effect of Subsonic Inlet Lip Geometry on Predicted Surface and Flow Mach Number Distributions," Technical Note to be published, NASA, Cleveland, Ohio.

17. Bober, L. J., "Use of Potential Flow Theory to Evaluate Subsonic Inlet Data," Technical Note to be published, NASA, Cleveland, Ohio.

18. Bergman, D., "Exhaust Nozzle Drag: Engine vs. Airplane Force Model," Paper 70-668, June 1970, AIAA, New York, N. Y.

$D_{MAX}/D_{FT} = 1.075$

$X_{OA}/D_{MAX} = 2.05$

$X_{FC}/D_{MAX} = 1.50$

PYLON t/c = 0.1125

$D_{FH}/D_{FT} = 0.40$

$D_{CORE}/D_{FT} = 0.425$

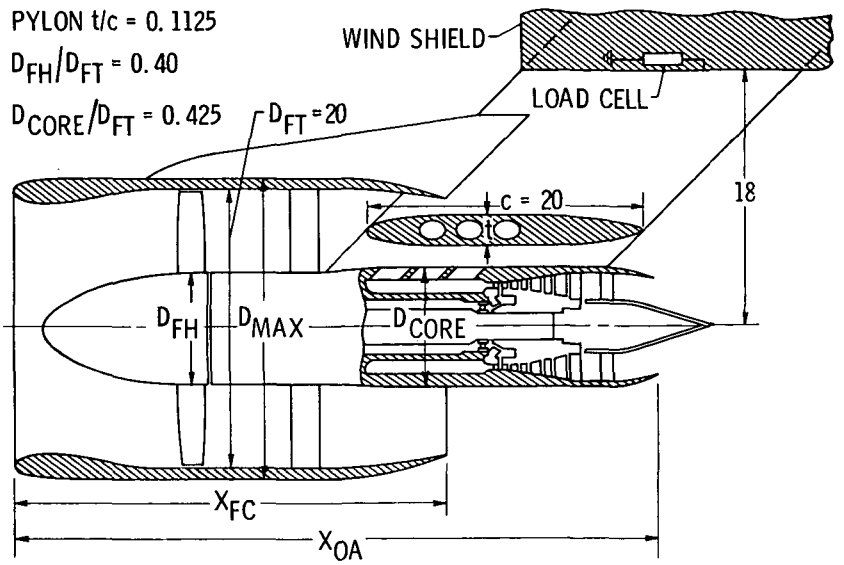

Figure 1. - Schematic view of 1.15 fan pressure ratio fan engine model. Dimensions (inches) are for cruise nacelle with inlet cowl No. 1.

E-7705

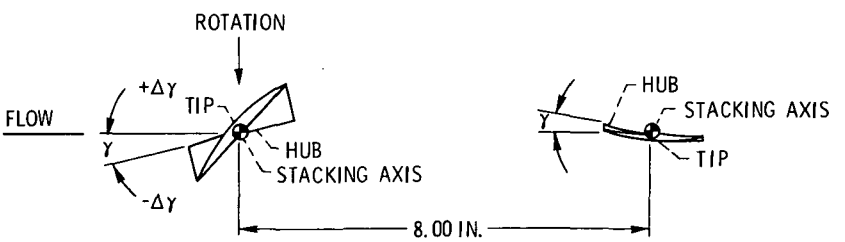

	ROTOR BLADE A	ROTOR BLADE B	STATOR BLADE
HUB CHORD, IN.	2.07	2.06	1.95
HUB DESIGN ANGLE, γ, DEG	13.0	12.7	9.3
HUB SOLIDITY	0.99	0.98	2.48
TIP CHORD, IN.	2.61	3.41	1.95
TIP DESIGN ANGLE, γ, DEG	48.0	50.3	5.1
TIP SOLIDITY	0.50	0.65	0.99
BLADE SECTION	DOUBLE CIRCULAR ARC		DOUBLE CIRCULAR ARC
BLADE ANGLE SETTING FOR FORWARD THRUST, Δγ, DEG			
LOW SPEED WIND TUNNEL	0	+3	----
HIGH SPEED WIND TUNNEL	+3	----	----

Figure 2. - Fan geometry.

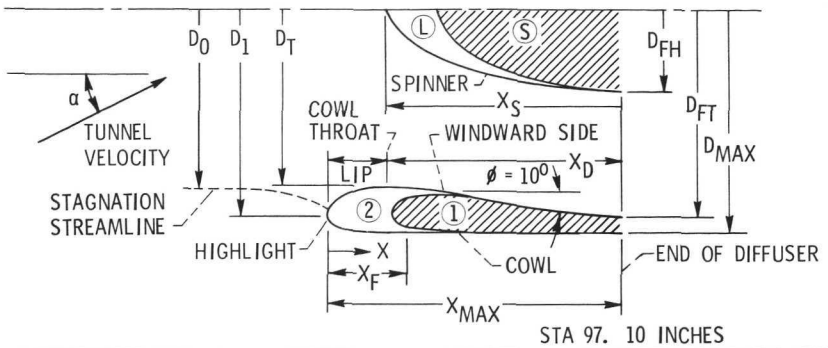

COWL	$\frac{D_1}{D_{MAX}}$	$\frac{X_F}{D_{MAX}}$	SPINNER	$\frac{X_S}{D_{MAX}}$	$\frac{A_1}{A_T}$	$\frac{A_1}{A_{MIN}}$	$\frac{X_D}{D_{MAX}}$	$\frac{X_{MAX}}{D_{MAX}}$	DIFFUSER EFFECTIVE CONE ANGLE DEGREES
1	0.935	0.175	(S) SHORT	0.414	1.26	1.30	0.414	0.516	6.5
1	.935	.175	(L) LONG	.530	1.26	1.37	.530	.516	9.2
2	.935	.175	(S) SHORT	.414	1.35	1.35	.414	.659	4.4
2	.935	.175	(L) LONG	.530	1.35	1.38	.530	.659	7.8

Figure 3. - Fan inlet geometry.

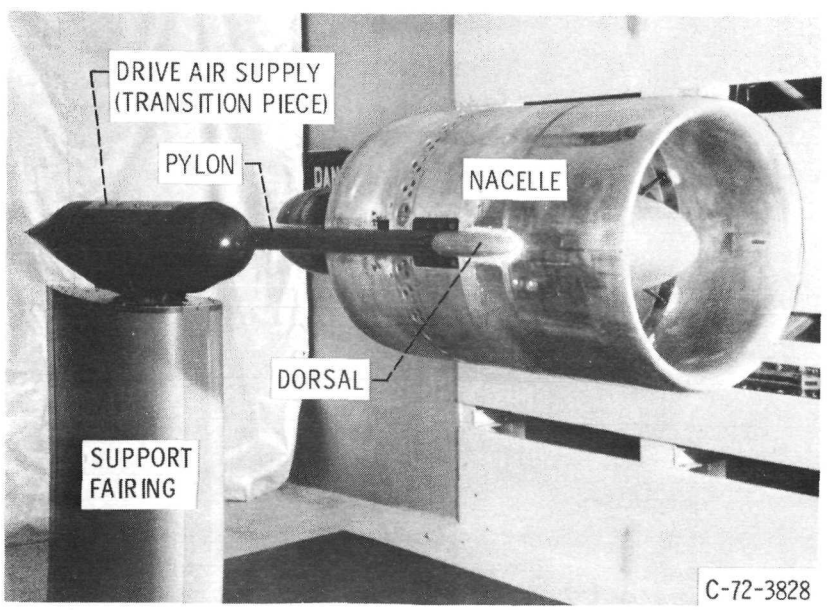

Figure 4. - Fan engine model in 9- by 15-Foot V/STOL Wind Tunnel.

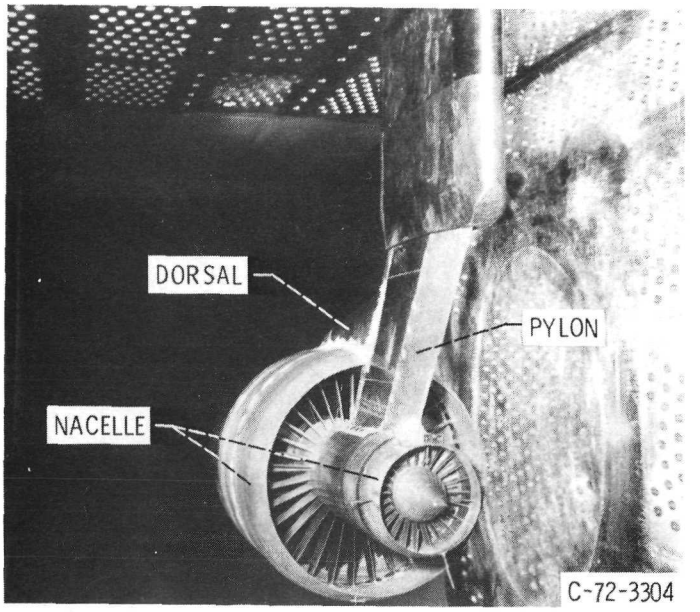

Figure 5. - Fan engine model in 8- by 6-Foot Supersonic Wind Tunnel.

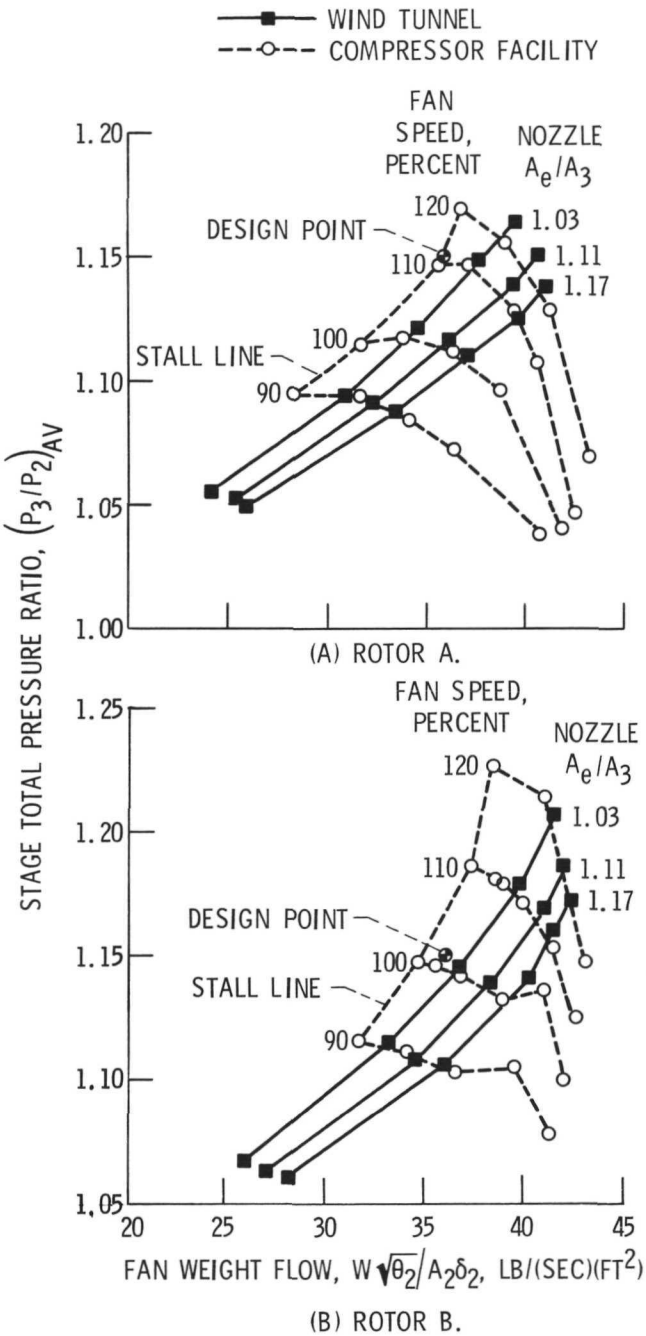

Figure 6. - Fan performance with various nozzles. Fan design speed, 9160 rpm; bellmouth inlet; long spinner; wind tunnel off.

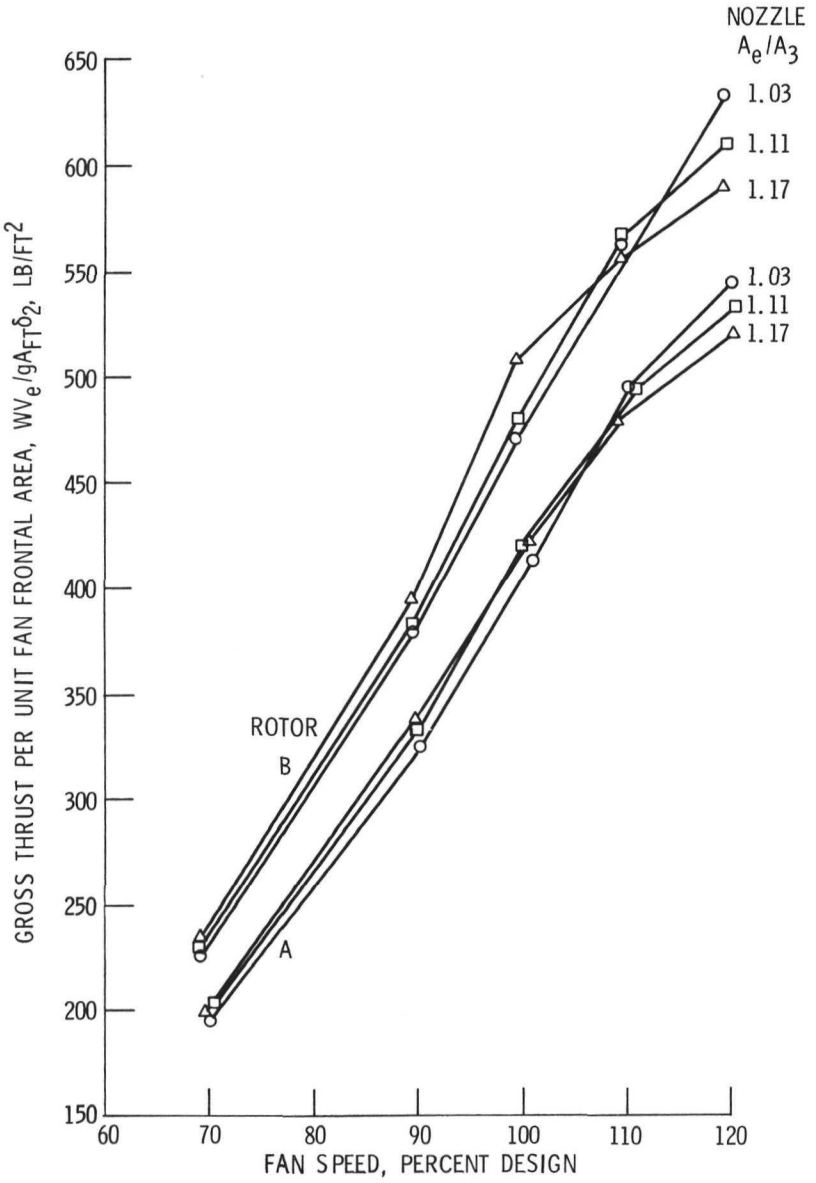

Figure 7. - Fan gross thrust with wind tunnel off. Bellmouth inlet, long spinner.

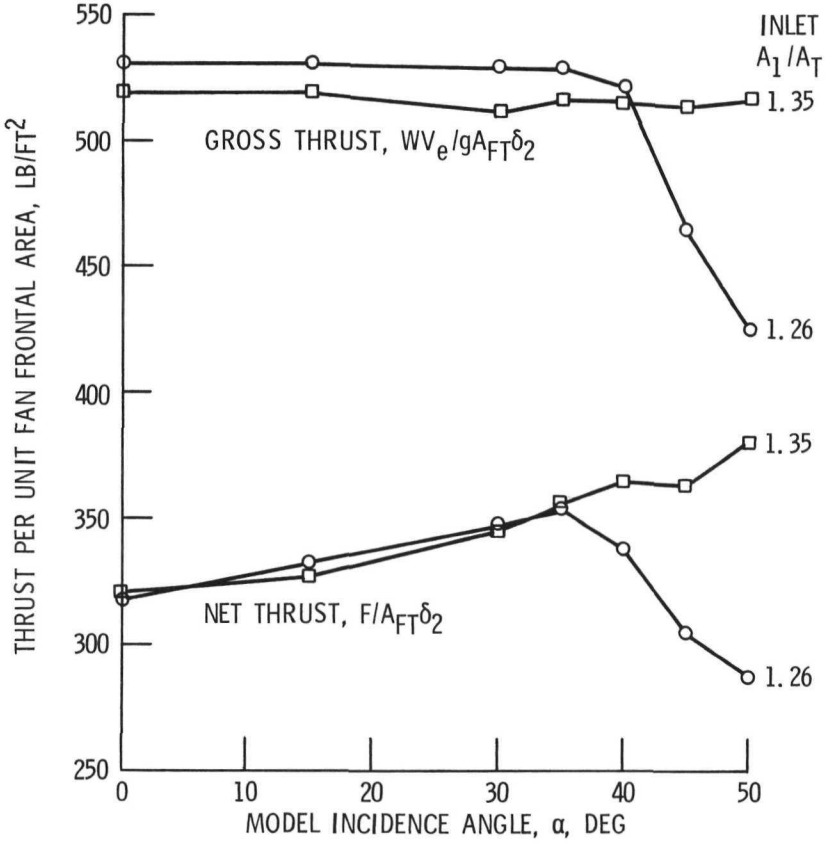

Figure 8. - Thrust performance for two inlets. Long spinner; nozzle, A_e/A_3, 1.17; rotor B at design speed; tunnel velocity, 143 ft/sec.

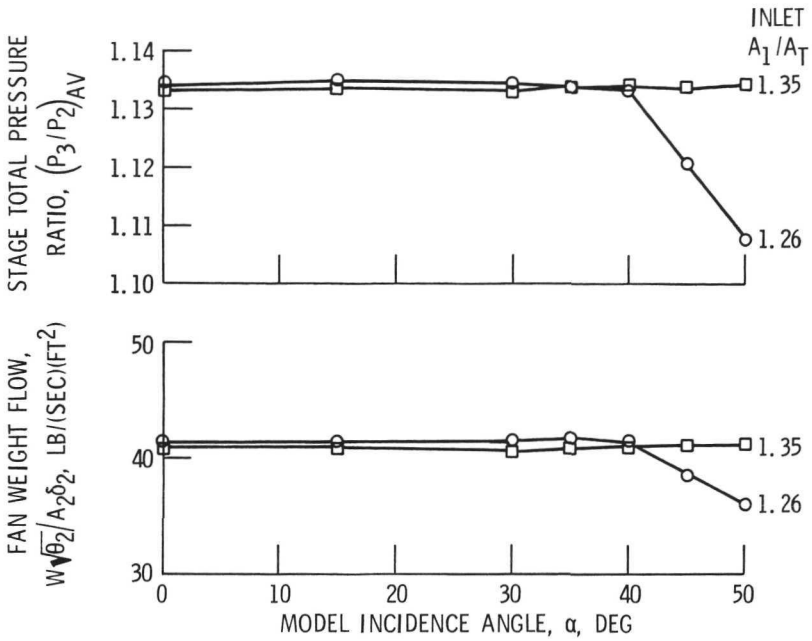

Figure 9. - Fan performance for two inlets. Long spinner; nozzle, A_e/A_3, 1.17; rotor B at design speed; tunnel velocity, 143 ft/sec.

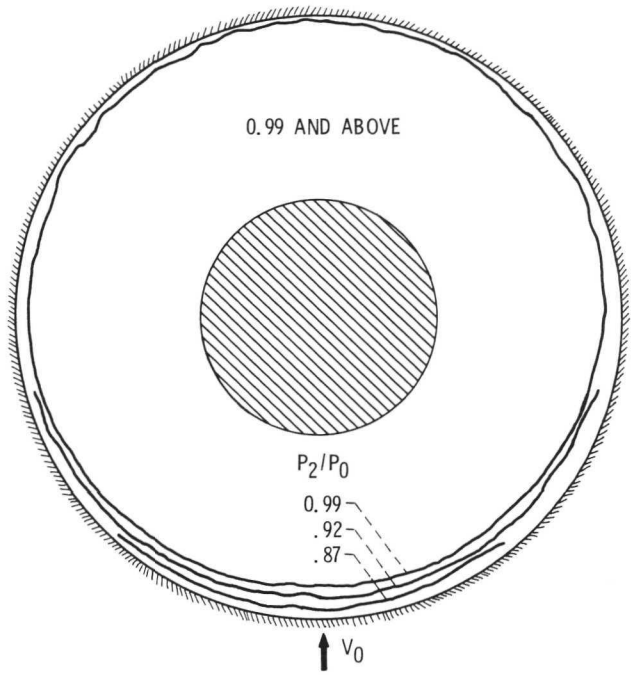

(A) INCIDENCE ANGLE, $\alpha = 30$ DEG. AVERAGE PRESSURE RECOVERY, $P_{2,AV}/P_0 = 0.993$; DISTORTION $\left(P_{2,MAX} - P_{2,MIN}\right)/P_{2,AV} = 0.098$, $\left(P_{2,AV} - P_{2,MIN60}\right)/P_{2,AV} = 0.008$.

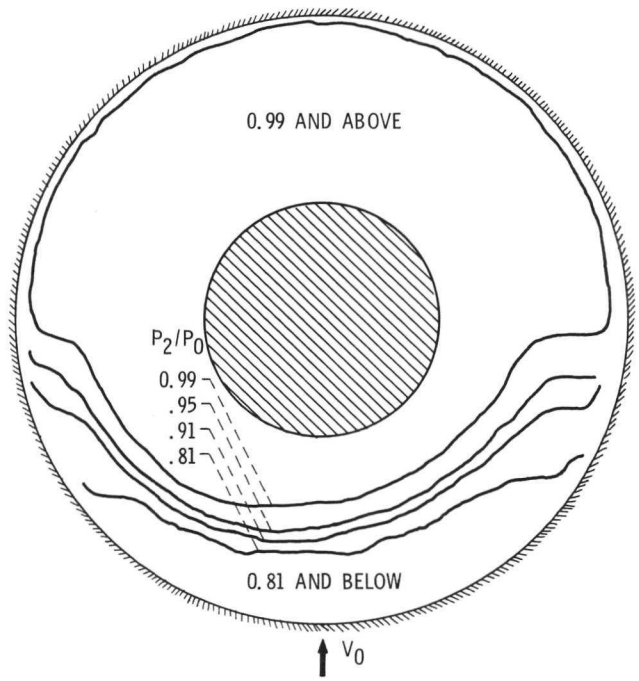

(B) INCIDENCE ANGLE, $\alpha = 50$ DEG. AVERAGE PRESSURE RECOVERY, $P_{2,AV}/P_0 = 0.958$; DISTORTION $\left(P_{2,MAX} - P_{2,MIN}\right)/P_{2,AV} = 0.326$, $\left(P_{2,AV} - P_{2,MIN60}\right)/P_{2,AV} = 0.103$.

Figure 10. - Fan face local pressure recovery contours. Inlet, A_1/A_T, 1.26, and long spinner; nozzle, A_e/A_3, 1.17; rotor B at design speed; tunnel velocity, 143 ft/sec.

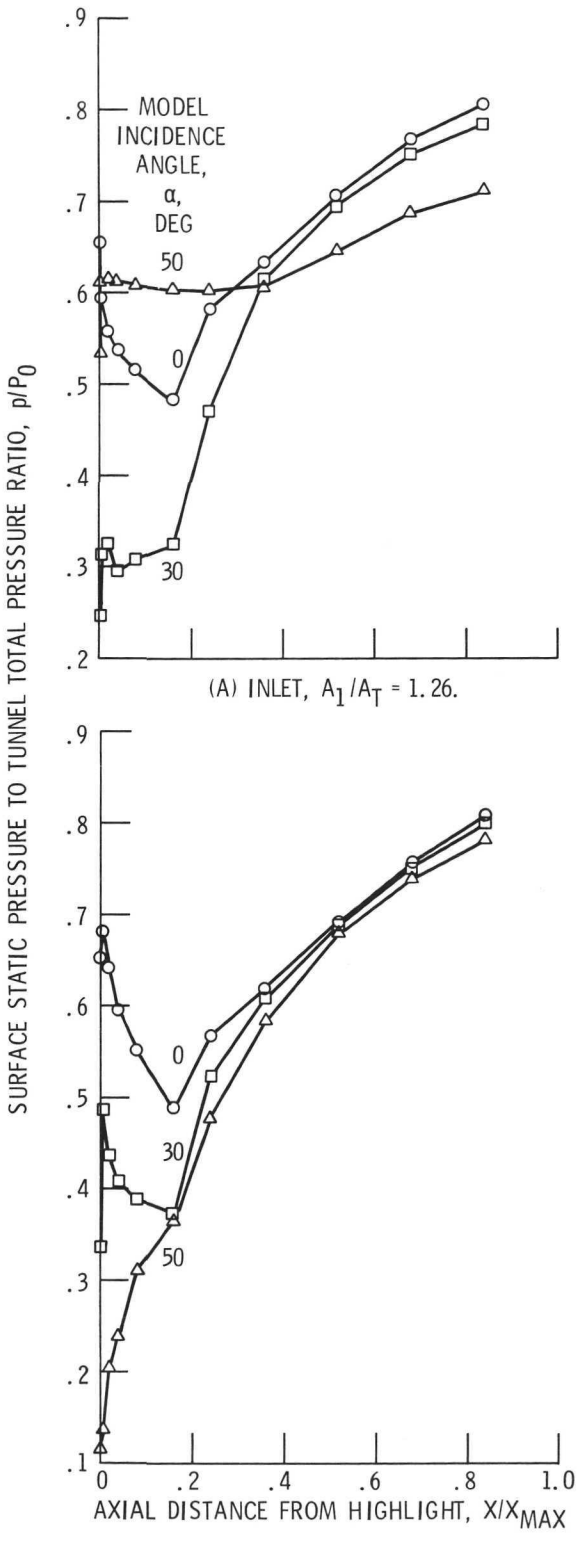

(A) INLET, A_1/A_T = 1.26.

(B) INLET, A_1/A_T = 1.35.

Figure 11. - Inlet duct windward side static pressure for two inlets. Long spinner; nozzle, A_e/A_3, 1.17; rotor B at design speed; tunnel velocity, 143 ft/sec.

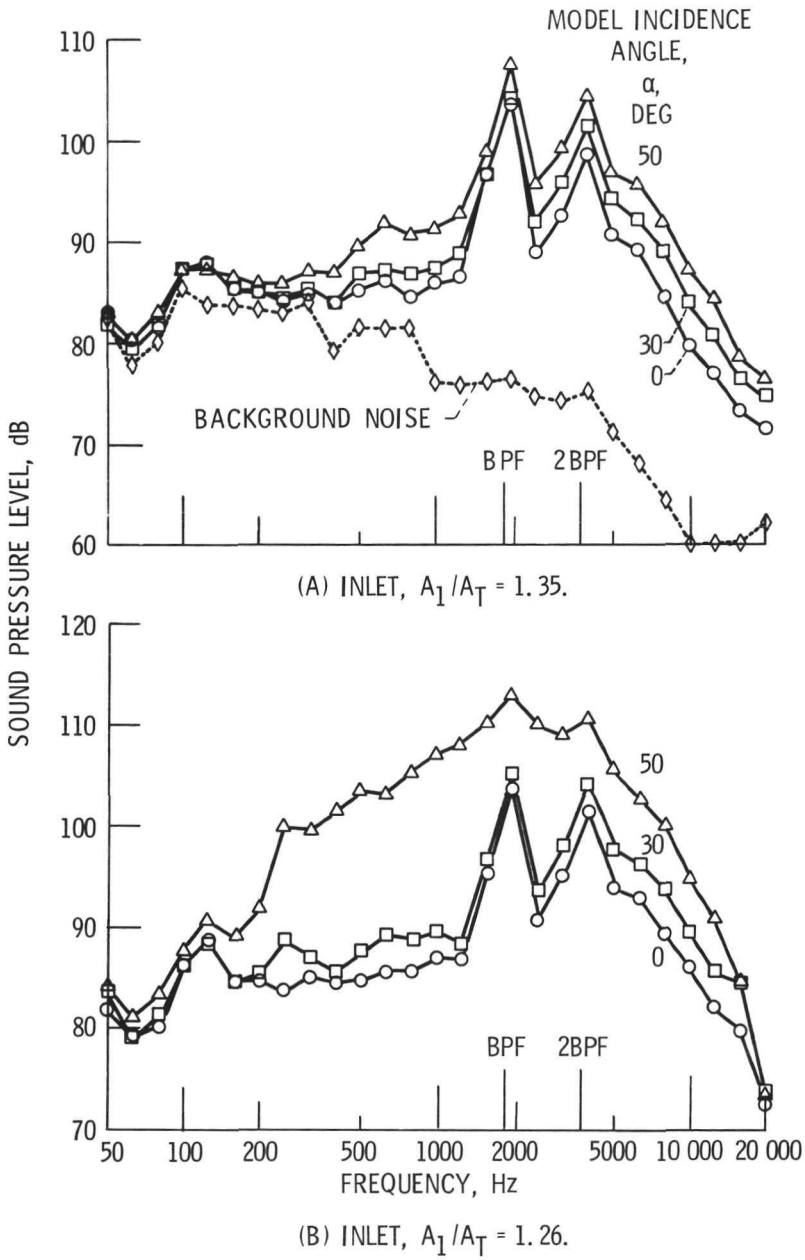

(A) INLET, $A_1/A_T = 1.35$.

(B) INLET, $A_1/A_T = 1.26$.

Figure 12. - Reverberant noise spectra for two inlets. Long spinner; nozzle, A_e/A_3, 1.17; rotor B at design speed; tunnel velocity, 143 ft/sec.

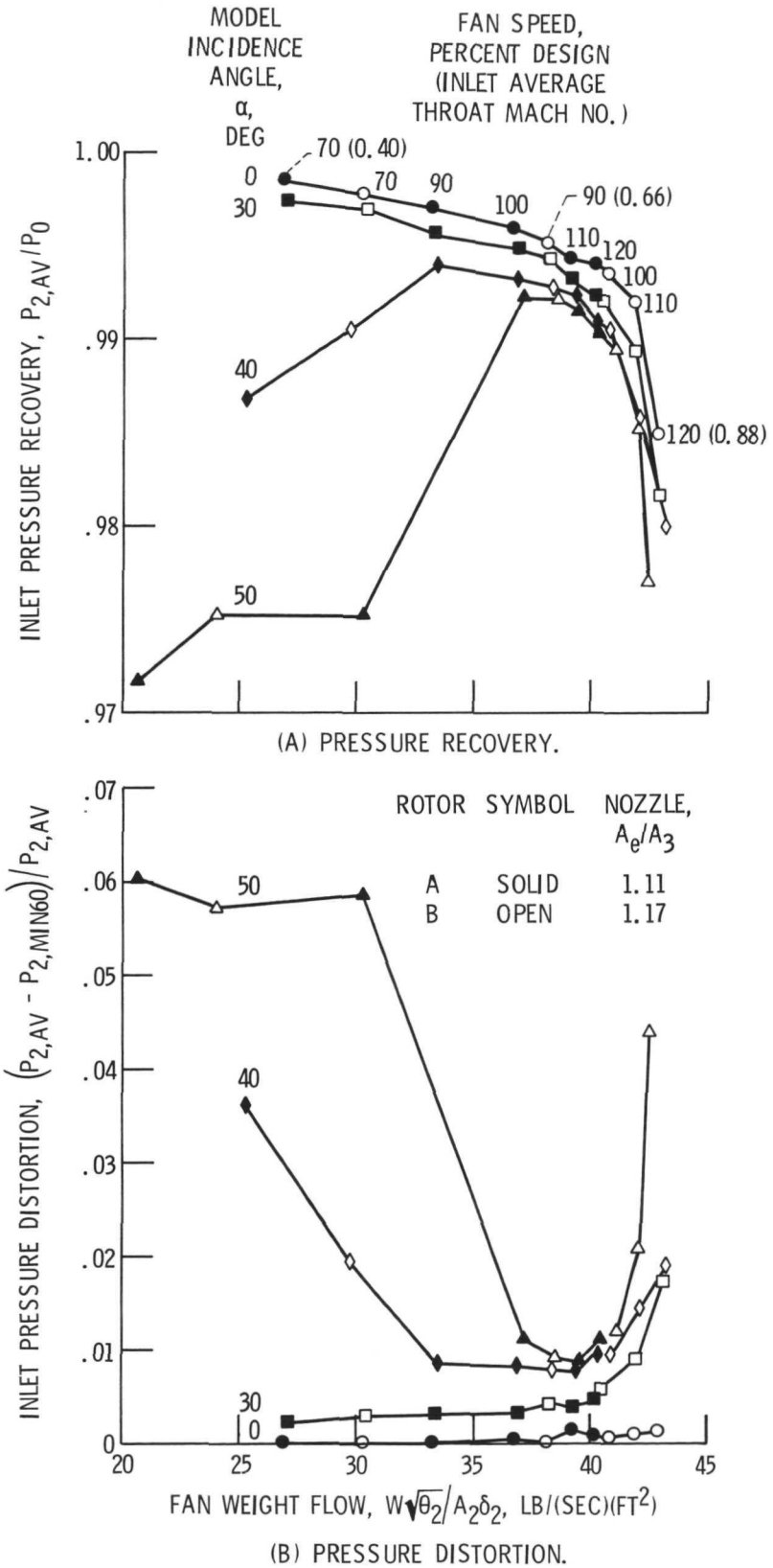

Figure 13. - Inlet performance for cowl, A_1/A_T, 1.35, and long spinner; tunnel velocity, 143 ft/sec.

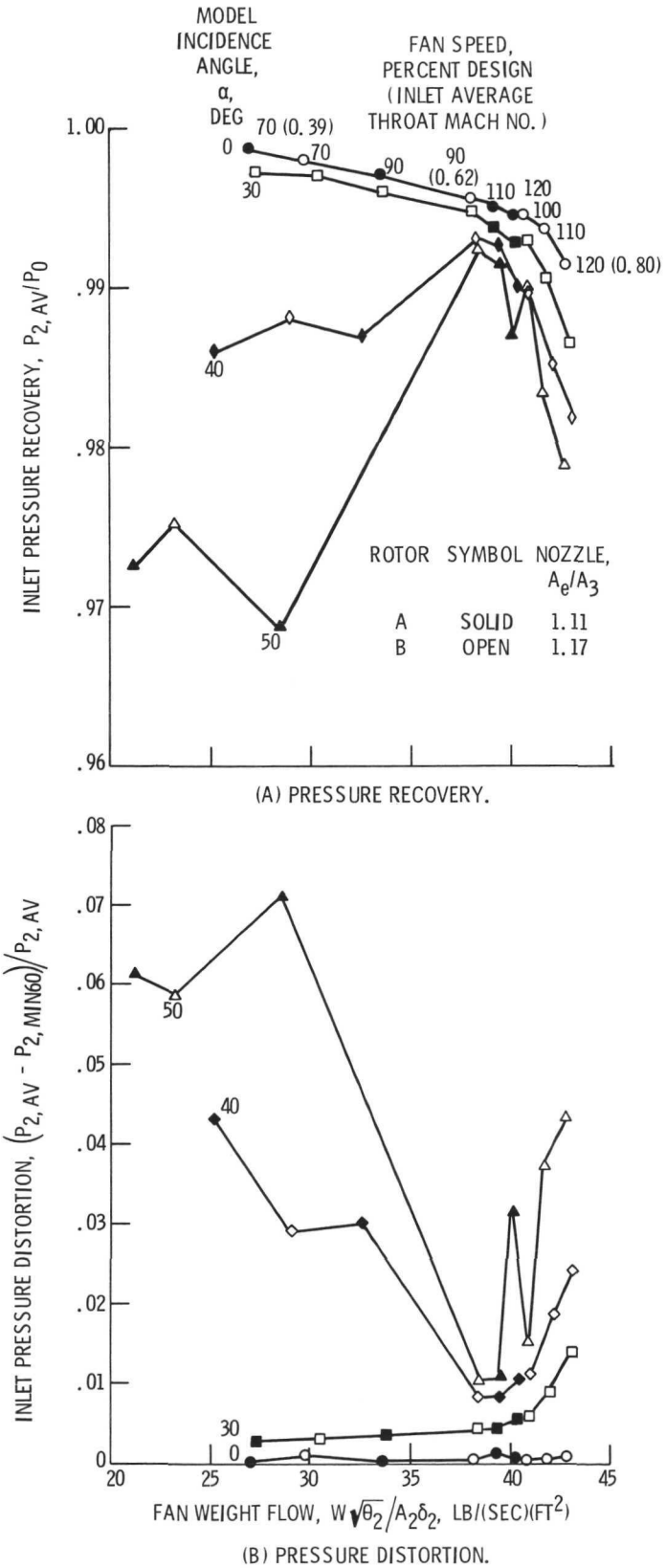

Figure 14. - Inlet performance for cowl, A_1/A_T, 1.35, and short spinner; tunnel velocity, 143 ft/sec.

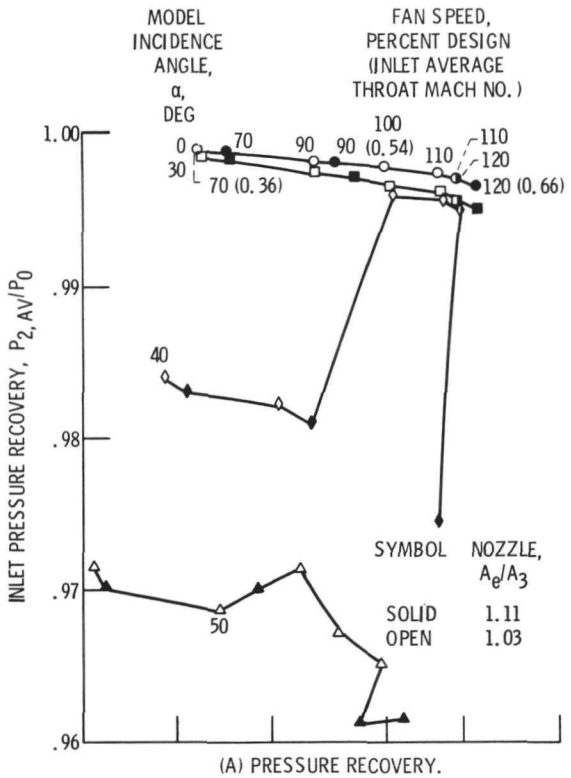

(A) PRESSURE RECOVERY.

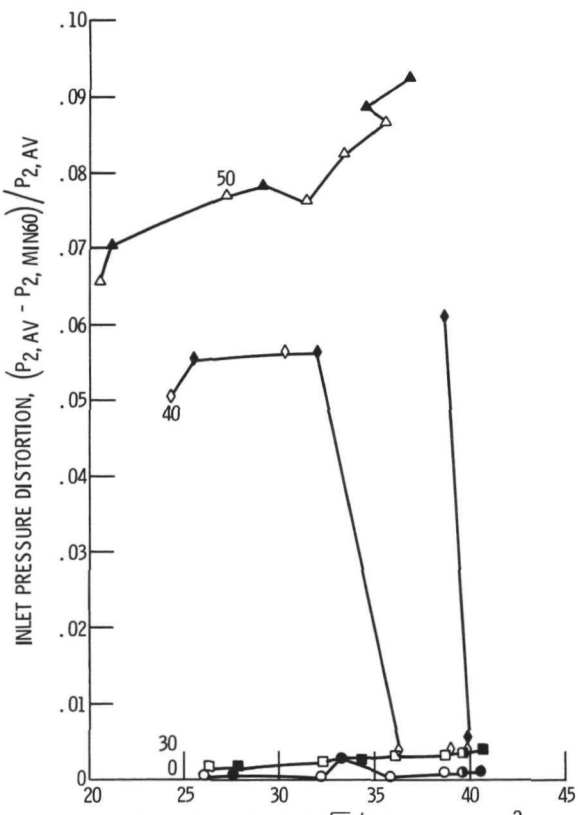

(B) PRESSURE DISTORTION.

Figure 15. - Inlet performance for cowl, A_1/A_T, 1.26, and short spinner; rotor A; tunnel velocity, 143 ft/sec.

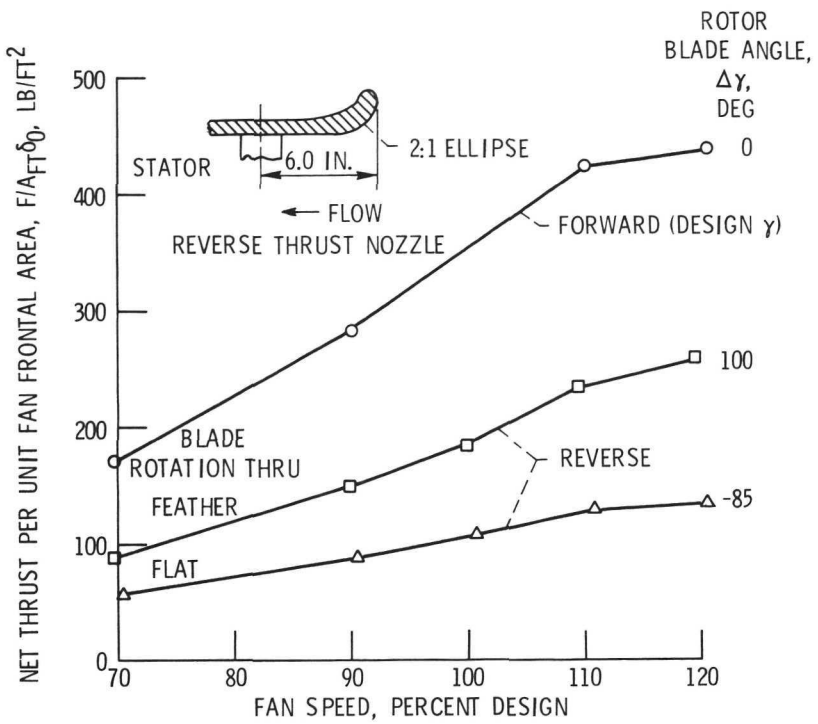

Figure 16. - Effect of rotor blade angle on fan net thrust. Rotor A; inlet cowl, A_1/A_T, 1.26, and short spinner; nozzle, A_e/A_3, 1.03 for forward thrust; bellmouth nozzle for reverse thrust; wind tunnel off.

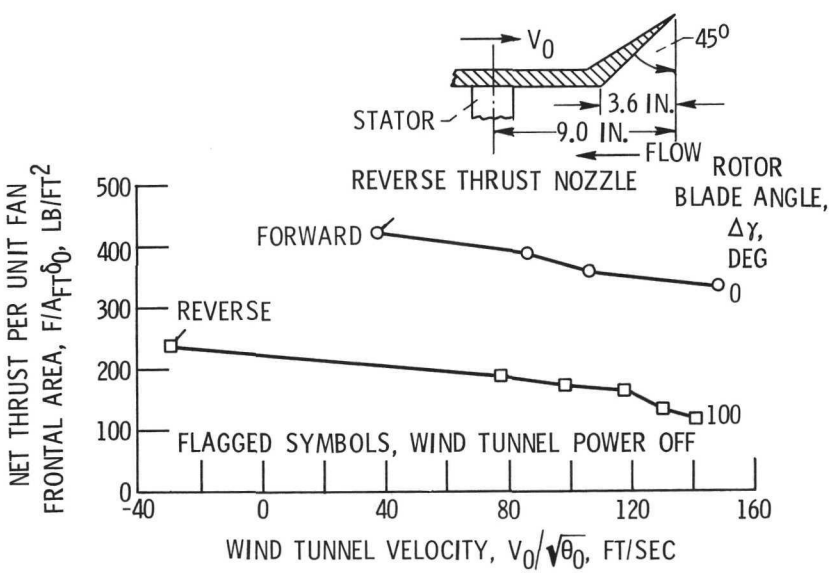

Figure 17. - Effect of wind tunnel velocity on fan net thrust. Rotor A at 110 percent design speed, inlet cowl, A_1/A_T, 1.26, and short spinner; nozzle, A_e/A_3, 1.03 for forward thrust; model incidence angle, α, 0 degrees.

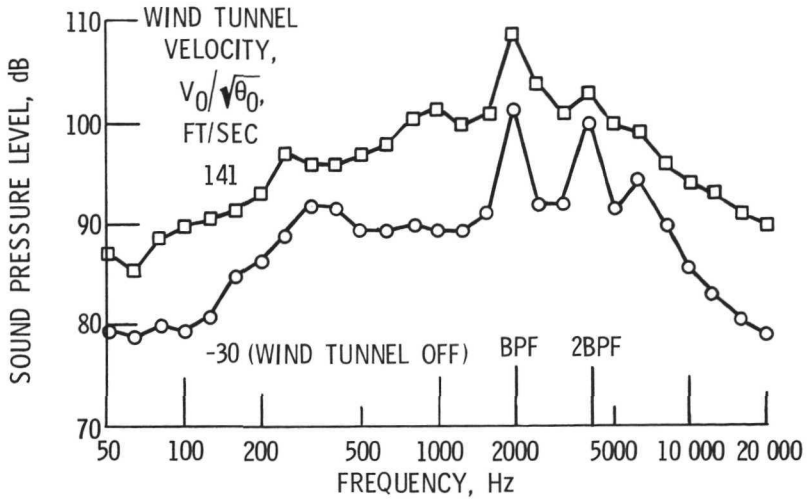

Figure 18. - Reverberant noise spectra for reverse thrust. Rotor A at 110 percent design speed and 100 degree blade angle, $\Delta\gamma$; inlet cowl, A_1/A_T, 1.26, and short spinner; reverse thrust nozzle (fig. 17); model incidence angle, α, 0 degrees.

E-7705

NOZZLE NO.	A_e, SQ. IN.	β, DEG	$R_{F\beta}/D_{MAX}$	D_{FE}/D_{MAX}
1	216.5	16.0	0.93	0.884
2	246.9	15.3	0.93	0.934

A_{ce}, SQ. IN.	$R_{c\beta}/D_{CORE}$	R_{CB}/D_{CORE}	D_{CE}/D_{CORE}
38.6	1.00	0.45	0.86

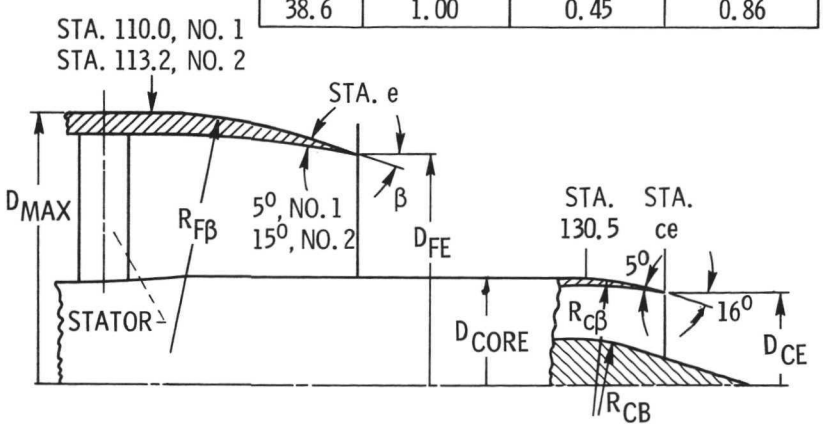

Figure 19. - Cruise nozzle geometry. Stations in inches.

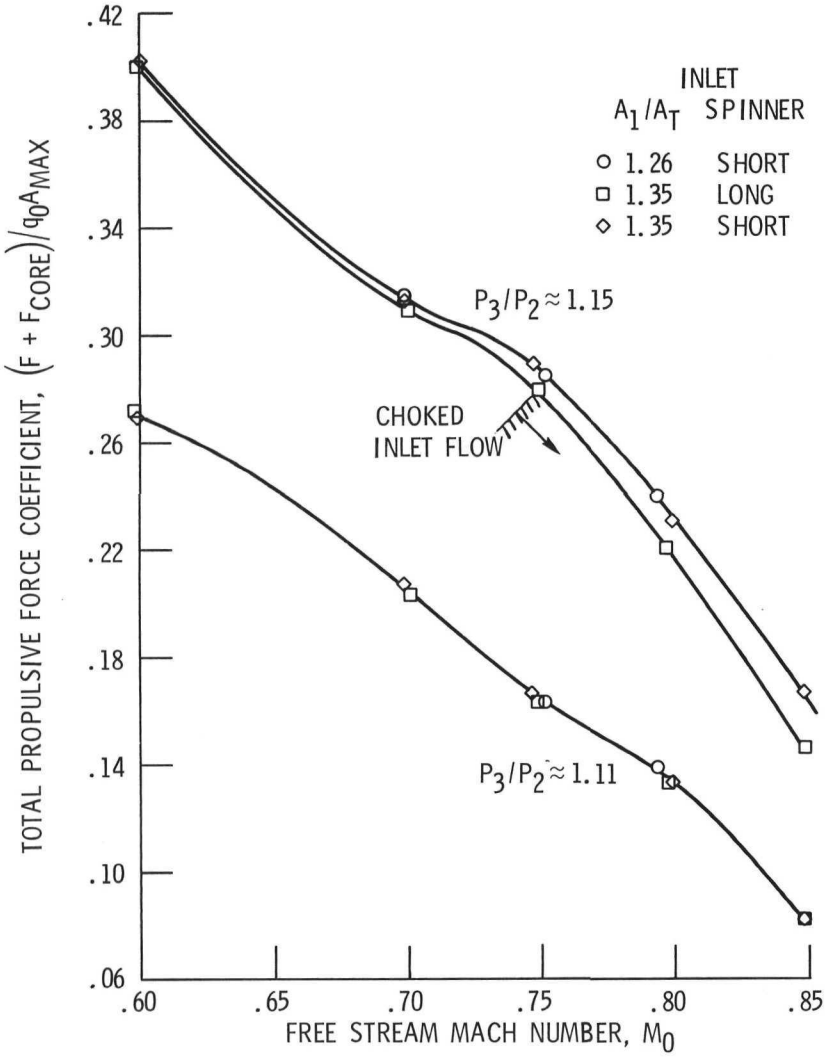

Figure 20. - Comparison of total propulsive force coefficients for three inlet configurations. Nozzle no. 1.

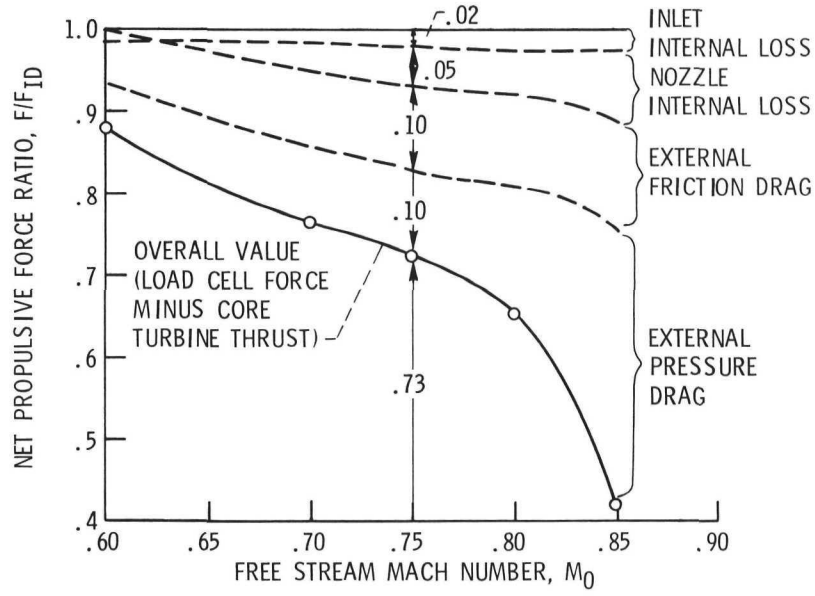

Figure 21. - Net propulsive force ratio and cruise loss breakdown of fan nacelle. Constant fan pressure ratio, P_3/P_2, 1.15; inlet, A_1/A_T, 1.26, and short spinner; nozzle no. 1.

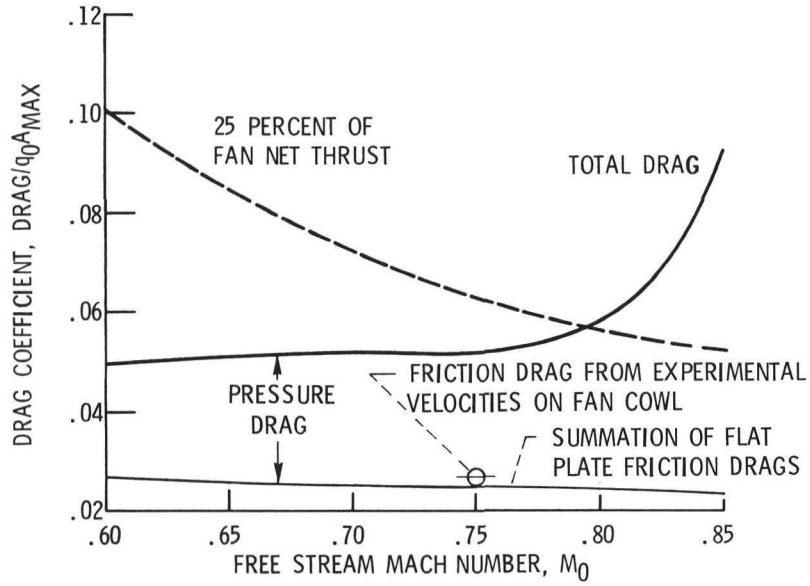

Figure 22. - Nacelle and pylon drag. Constant fan pressure ratio, P_3/P_2, 1.15; inlet, A_1/A_T, 1.26, and short spinner; fan nozzle no. 1.

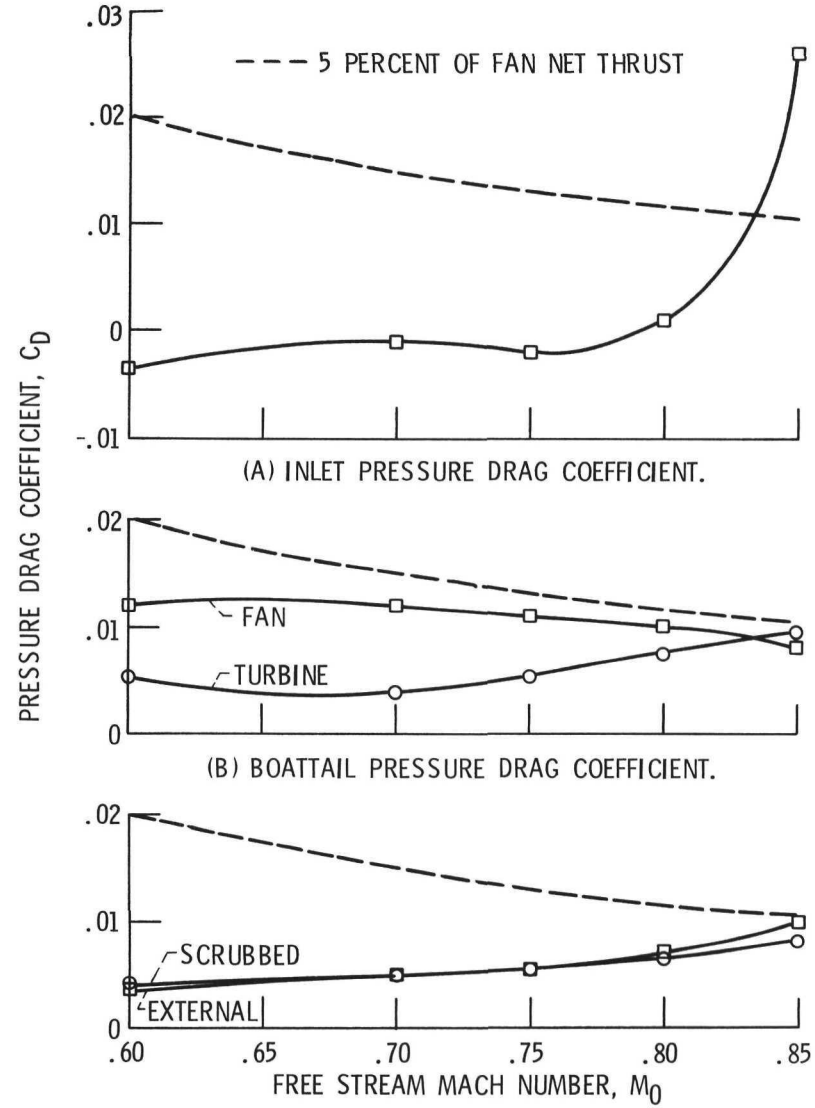

Figure 23. - Nacelle component pressure drags. Constant fan pressure ratio, P_3/P_2, 1.15; inlet, A_1/A_T, 1.26, and short spinner; nozzle no. 1.

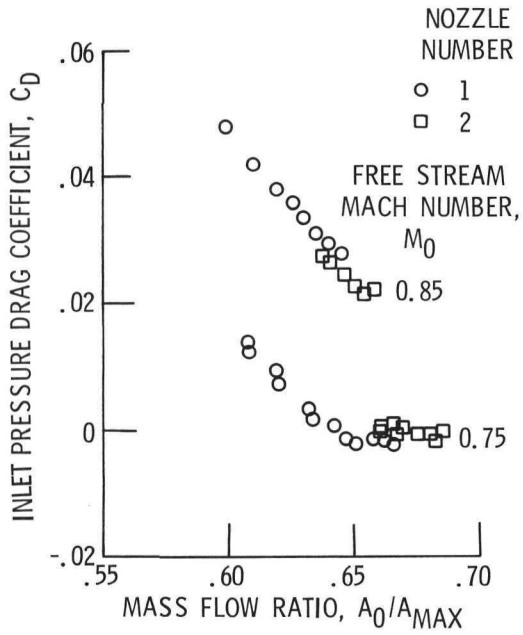

Figure 24. - Variation of inlet pressure drag with mass flow ratio. Inlet, A_1/A_T, 1.26, and short spinner.

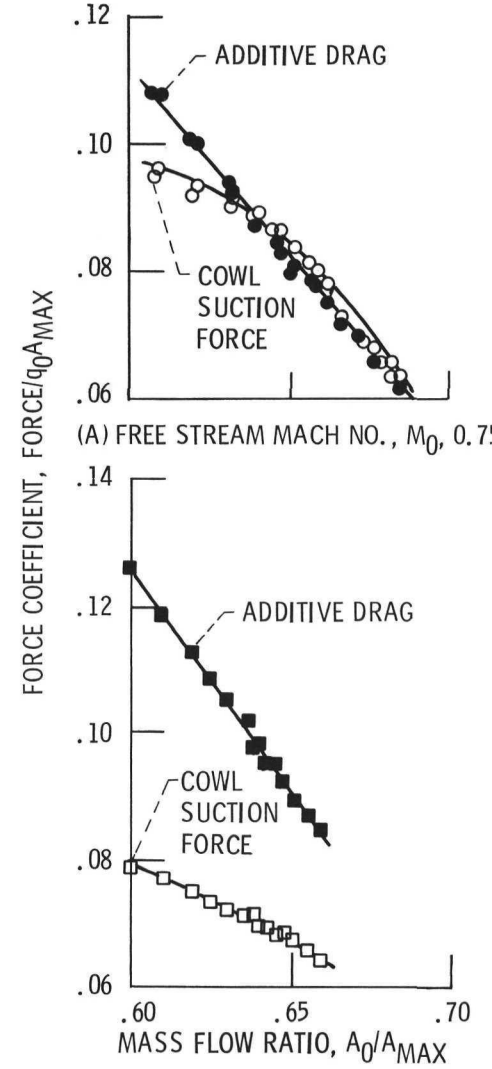

(A) FREE STREAM MACH NO., M_0, 0.75.

(B) FREE STREAM MACH NO., M_0, 0.85

Figure 25. - Variation of cowl suction force and additive drag coefficients with inlet mass flow ratio; inlet, A_1/A_T, 1.26, and short spinner; nozzle no. 1 and 2.

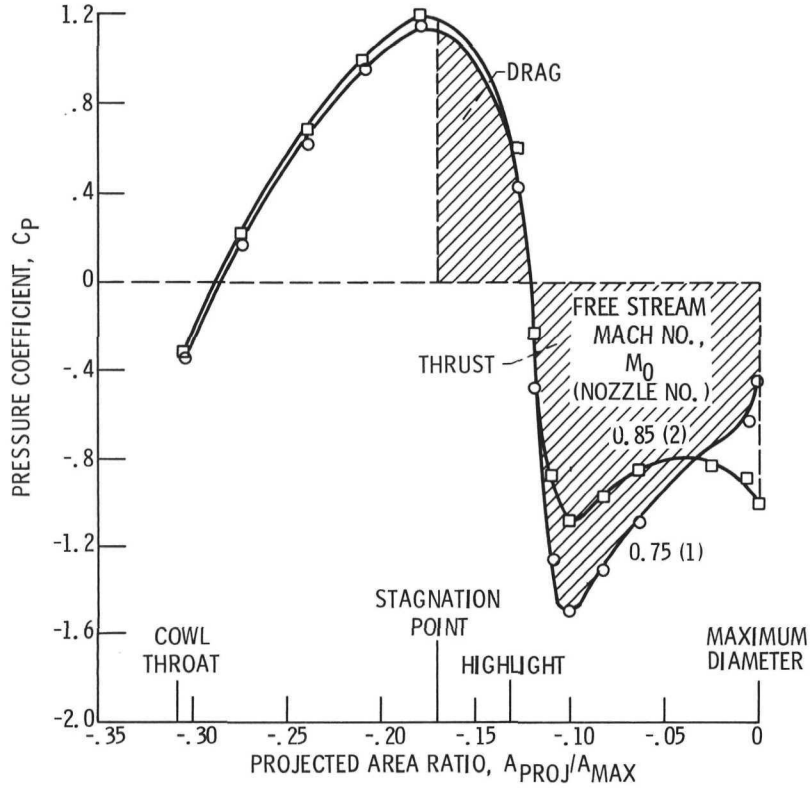

Figure 26. - Inlet pressure coefficient distributions at a mass flow ratio, A_0/A_{MAX}, 0.658; inlet, A_1/A_T, 1.26, and short spinner.

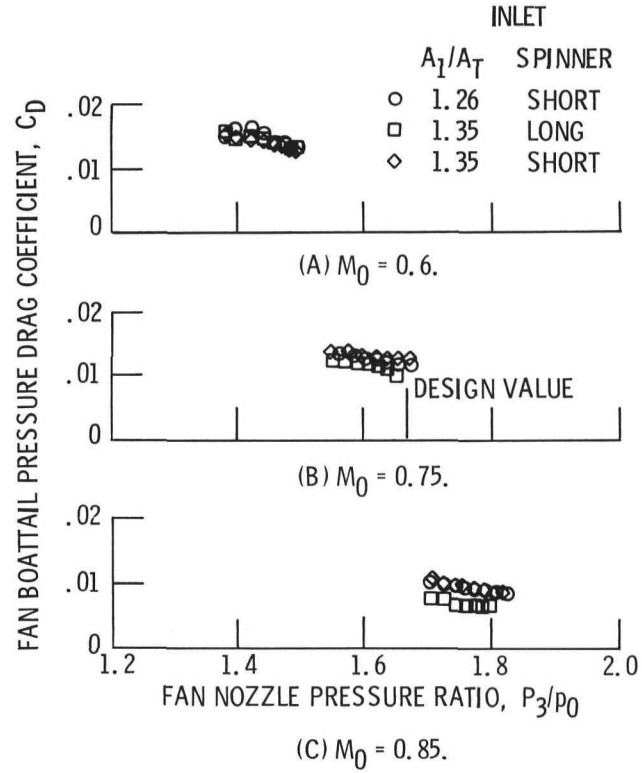

Figure 27. - Boattail pressure drag coefficients for fan nozzle 1 with various inlets.

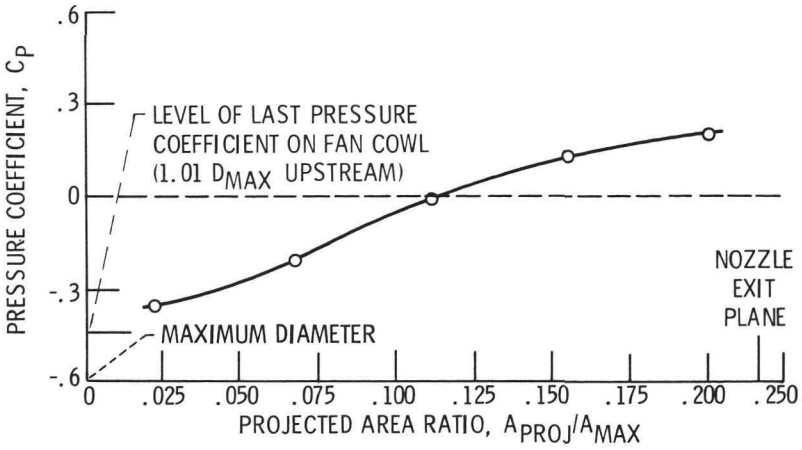

Figure 28. - Pressure coefficient profiles for fan boattail no. 1; inlet, A_1/A_T, 1.26, and short spinner; free stream Mach no., M_0, 0.75; nozzle pressure ratio, P_3/p_0, 1.67.

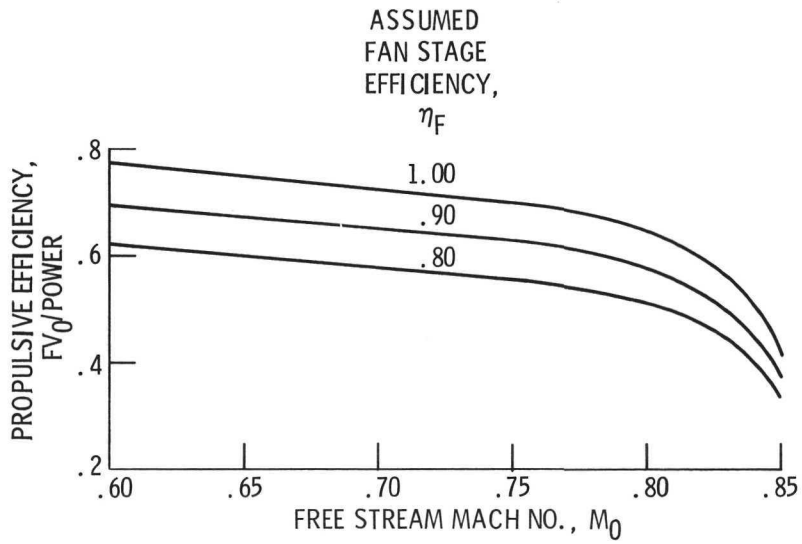

Figure 29. - Propulsive efficiency of fan/nacelle system; constant fan pressure ratio, P_3/P_2, 1.15; fan weight flow, $W\sqrt{\theta_2}/\delta_2 A_{MAX}$, 30.1 lb/(sec)(ft^2); inlet, A_1/A_T, 1.26, and short spinner; nozzle no. 1.

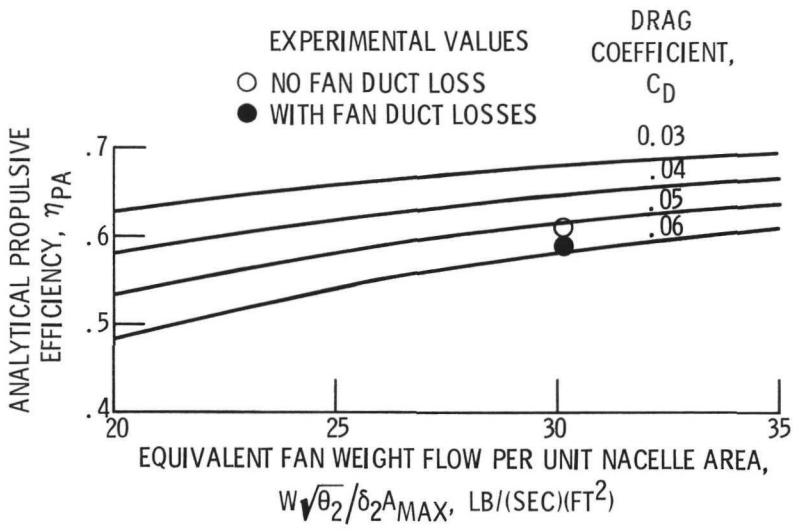

Figure 30. - Effect of equivalent fan weight flow per unit nacelle area on the propulsive efficiency of a 1.15 pressure ratio fan/nacelle system for several levels of nacelle drag coefficient. $M_0 = 0.75$, $\eta_F = 0.85$.